

Radiative Dirac Neutrino Masses from Modular S_3 Symmetry in an Axion Model

Sin Kyu Kang,^{1,*} Ranjeet Kumar,^{2,†} and Hiroshi Okada^{3,‡}

¹*Seoul National University of Science and Technology, Seoul 01811, Republic of Korea*

²*Institute for Convergence of Basic Studies,*

Seoul National University of Science and Technology, Seoul 01811, Republic of Korea

³*Department of Physics, Henan Normal University, Xinxiang 453007, China*

We present a unified axion model framework that simultaneously addresses the origin of neutrino masses, leptonic flavor structure, the strong CP problem, and dark matter. The model is based on a global $U(1)_{\text{PQ}}$ symmetry combined with a modular S_3 symmetry and is realized within a novel class of KSVZ-type axion model. Exotic colored fermions and scalars mediate radiative neutrino mass generation at the one loop-level. The PQ charge assignment forbids tree-level neutrino masses and leaves a residual Z_3 symmetry that ensures the Dirac nature of neutrinos. In the minimal realization, the neutrino mass matrix is of rank two, predicting one massless neutrino. Consequently, the sum of neutrino masses is constrained for both the normal and inverted hierarchies. We analyze the implications for charged lepton flavor violation and the lepton $g - 2$. The axion emerging from this framework dynamically resolves the strong CP problem and accounts for the observed dark matter abundance. Notably, the predicted axion-photon coupling is within reach of upcoming experiments and consistent with existing astrophysical and cosmological bounds.

1. INTRODUCTION

The experimental confirmation of neutrino oscillations has firmly established that neutrinos possess nonzero masses and undergo flavor mixing [1–5]. At the same time, a wide

* skkang@seoultech.ac.kr

† kumarranjeet.drk@gmail.com

‡ hiroshi3okada@htu.edu.cn

range of astrophysical and cosmological observations indicate that nearly 85% of the matter content of the Universe is composed of dark matter (DM) [6]. These observations highlight the limitations of the Standard Model (SM), which lacks both a mechanism for neutrino mass generation and a viable DM candidate and thus point to physics beyond the SM (BSM). Therefore, extensions of the SM that simultaneously address neutrino masses and DM within a single framework are particularly appealing. Among such approaches, the scotogenic model [7] provides a simple and elegant framework in which neutrino masses arise radiatively and are intimately connected to DM phenomenology. Numerous variants of scotogenic models have been proposed, realizing neutrinos as either Majorana or Dirac particles [8–36].

Another longstanding puzzle in particle physics is the apparent absence of CP-violation in Quantum Chromodynamics (QCD). Experimental constraints require the CP-violating parameter $\bar{\theta}$ to be extremely small, $|\bar{\theta}| < 10^{-10}$ [37, 38]. This tension constitutes the strong CP problem, raising the fundamental question of why CP symmetry is strongly violated in the weak interactions while it appears to be preserved in the strong force. The strong CP problem can be naturally resolved within the Peccei-Quinn (PQ) framework [39, 40] through the introduction of a new global symmetry denoted as $U(1)_{\text{PQ}}$. The spontaneous breaking of this symmetry gives rise to a pseudo-Goldstone boson known as the axion [41, 42]. Once the PQ symmetry is spontaneously broken, it induces an effective term with the same structure as the QCD $\bar{\theta}$ -term. As a result, the CP-violating phase $\bar{\theta}$ is promoted to a dynamical axion field, whose vacuum minimum effectively leads $\bar{\theta}$ to be zero, thereby resolving the strong CP problem. Well studied axion models such as KSVZ [43, 44] and DFSZ [45, 46] provide distinct realizations of the PQ mechanism, characterized by different PQ charge assignments to SM quarks and additional heavy fermions.

Most theoretical efforts have focused on resolving these puzzles separately by introducing distinct new particles or symmetries for each phenomenon. However, recently, a KSVZ-type axion model has been proposed that simultaneously addresses neutrino mass generation, the strong CP problem, and the DM phenomenology within a unified framework [47]. In this setup, neutrino masses are generated radiatively at the one loop-level, following a mechanism analogous to that of the scotogenic model [7]. A similar idea has also been explored for the two-loop neutrino mass generation [48, 49]. These constructions also exploit the fact that axion can also serve as a viable cold DM candidate [50–52].

In this work, we introduce a KSVZ-type axion model framework in which neutrino mass generation, the strong CP problem, and DM phenomenology are addressed in a unified manner at the one loop-level. In addition, the leptonic flavor structure emerges from an underlying modular S_3 symmetry, providing a predictive setup for neutrino mixing¹. We have introduced the vector-like fermions (Ψ_{L_i}, Ψ_{R_i}) , scalar χ , singlets under $SU(2)_L$ and scalar η , doublet of $SU(2)_L$. They are triplets under the fundamental representation of $SU(3)_C$ and singlets of modular S_3 symmetry carrying -2 modular weight. In addition, we consider a global $U(1)_{\text{PQ}}$ symmetry, whose spontaneous breaking leads to the axion. This provides a solution to the strong CP problem as well as a promising axion DM candidate. The $U(1)_{\text{PQ}}$ symmetry is spontaneously broken by the vacuum expectation value (vev) of the newly added complex scalar σ . Except for the Higgs field H , all fields in the model carry non-trivial PQ charges. Moreover, the PQ charge assignment forbids neutrino masses at the tree level, and the breaking of $U(1)_{\text{PQ}}$ leads to a residual Z_3 symmetry, which ensures the Dirac nature of neutrinos. We consider the effective operator $\bar{L}\tilde{H}\nu_R\sigma^*$ for Dirac neutrino mass generation, whose ultra-violate (UV) completion is realized by the colored fields, $\Psi_{L_i}, \Psi_{R_i}, \chi$, and η at the one loop-level.

The remainder of the paper is organized as follows. In Sec. 2, we introduce our model framework and discuss the scalar sector and its mass spectrum, as well as derive the charged lepton and neutrino mass matrices. We discuss the numerical analysis in Sec. 3 and present our model's predictions for both the normal hierarchy (NH) and inverted hierarchy (IH) of neutrino masses. In Sec. 4, we analyze the charged lepton flavor violation (cLFV) and comment on the lepton $g - 2$ based on our numerical analysis. A detailed discussion of the axion as a solution to the strong CP problem, a viable DM candidate, and axion-photon coupling is provided in Sec. 5. Finally, we give our concluding remarks in Sec. 6.

2. MODEL FRAMEWORK

We consider a model framework where Dirac neutrino mass generation is interconnected with the axion. The effective operator $\bar{L}\tilde{H}\nu_R\sigma^*$ has been considered in conjunction with modular S_3 symmetry for the Dirac neutrino mass generation and mixing. Similar to the

¹ Modular symmetry has recently emerged as a compelling framework, in which the usual discrete flavor symmetries are generalized to modular symmetries [53], where Yukawa couplings are promoted to modular forms that transform non-trivially under the modular group, resulting in predictive lepton and/or quark mixing patterns [54–98].

original KSVZ models [43, 44], we introduce vector-like fermions Ψ_L and Ψ_R . These are triplets in the fundamental representation of $SU(3)_C$, singlets under $SU(2)_L$, and have hypercharge $Y = 0$. In the minimal realization of the model, we consider two generations of Ψ_{L_i} and Ψ_{R_i} ($i = 1, 2$). As a consequence, only two neutrinos acquire nonzero masses, while one remains massless, consistent with neutrino oscillation data [1–5]. We further incorporate a $U(1)_{\text{PQ}}$ symmetry, which serves multiple purposes within our model. The $U(1)_{\text{PQ}}$ charge assignment of left handed lepton doublet L and right handed neutrino ν_R forbids the tree-level mass terms. In addition, the $U(1)_{\text{PQ}}$ charges have been chosen in such a way that the breaking of $U(1)_{\text{PQ}}$ symmetry leads to the residual Z_3 symmetry: $U(1)_{\text{PQ}} \rightarrow Z_3$. This residual symmetry ensures the Dirac nature of neutrinos and forbids Majorana mass terms. Earlier, this has been explored in the context of $U(1)_{B-L} \rightarrow Z_N$ [30, 99–101]. The spontaneous breaking of $U(1)_{\text{PQ}}$ is achieved via a newly added complex scalar singlet σ , which also generates masses for the vector-like fermions. The phase of scalar σ corresponds to the axion field a . Assigning different PQ charges to Ψ_{L_i} and Ψ_{R_i} ensures the anomalous axion-gluon coupling responsible for addressing the strong CP problem.

These vector-like fermions also serve as mediators for neutrino mass generation at the one loop-level. To UV-complete the operator $\bar{L} \tilde{H} \nu_R \sigma^*$, two additional scalars, η and χ are introduced, which are triplets under the fundamental representation of $SU(3)_C$. The scalar η (χ) is an $SU(2)_L$ doublet (singlet) with $Y = 1/2$ ($Y = 0$). The PQ charge assignments of the fields propagating in the loop are parametrized by a free parameter q , which denotes the charge of Ψ_{R_i} . Furthermore, under the modular S_3 symmetry, only leptons $L_{23} \equiv (L_2, L_3)^T$, $e_{R_{23}} \equiv (e_{R_2}, e_{R_3})^T$, and right handed neutrino $\nu_{R_{23}} \equiv (\nu_{R_2}, \nu_{R_3})^T$ are assigned doublets **(2)**, while Ψ_{L_2} , Ψ_{R_2} are singlets **(1')**, and all the remaining fields of the model are assigned trivial singlet **(1)** under S_3 . The modular weight assignments are such that $e_{R_{23}}$, $\nu_{R_{23}}$, H , and σ are assigned weight 0, while the remaining fields have weight -2 . The field content and their transformation properties under the different symmetries, along with the modular weights, are summarized in Table I.

In what follows, we construct the most general renormalizable Lagrangian consistent with $SU(3)_C \otimes SU(2)_L \otimes U(1)_Y$, the global $U(1)_{\text{PQ}}$, and the modular S_3 symmetry. The τ -dependence of selected parameters is treated effectively, motivated by modular invariance, without committing to a specific UV-complete supersymmetric model.

	Fermions										Bosons			
	L_1	L_{23}	e_{R_1}	$e_{R_{23}}$	ν_{R_1}	$\nu_{R_{23}}$	Ψ_{L_1}	Ψ_{L_2}	Ψ_{R_1}	Ψ_{R_2}	H	η	σ	χ
$SU(3)_C$	1	1	1	1	1	1	3	3	3	3	1	3	1	3
$SU(2)_L$	2	2	1	1	1	1	1	1	1	1	2	2	1	1
$U(1)_Y$	$-\frac{1}{2}$	$-\frac{1}{2}$	-1	-1	0	0	0	0	0	0	$\frac{1}{2}$	$\frac{1}{2}$	0	0
$U(1)_{\text{PQ}}$	$\frac{1}{6}$	$\frac{1}{6}$	$\frac{1}{6}$	$\frac{1}{6}$	$\frac{2}{3}$	$\frac{2}{3}$	$q + \frac{1}{2}$	$q + \frac{1}{2}$	q	q	0	$q - \frac{1}{6}$	$\frac{1}{2}$	$q - \frac{1}{6}$
S_3	1	2	1	2	1	2	1	$1'$	1	$1'$	1	1	1	1
$-k$	$\overline{-2}$	$\overline{-2}$	-2	0	-2	0	$\overline{-2}$	$\overline{-2}$	-2	-2	0	$\overline{-2}$	0	-2

TABLE I: Field content and transformation properties of different fields under the $SU(3)_C \otimes SU(2)_L \otimes U(1)_Y \otimes U(1)_{\text{PQ}} \otimes S_3$ symmetry. Here, $-k$ denotes the modular weight and $\overline{-2}$ for the left handed fermions ψ' s $\equiv \{L_1, L_{23}, \Psi_{L_1}, \Psi_{L_2}\}$ and η is defined so that -2 is for $\overline{\psi}'s$ and $\tilde{\eta}$.

2.1. Scalar Sector and the Resulting Mass Spectrum

Following the charge assignments of the fields under the various symmetries given in Table I, the scalar potential of the model can be formulated as

$$\begin{aligned} \mathcal{V} = & -\mu_H^2 |H|^2 + \boldsymbol{\mu}_\eta^2 |\eta|^2 + \boldsymbol{\mu}_\chi^2 |\chi|^2 - \mu_\sigma^2 |\sigma|^2 + \lambda_H |H|^4 + \lambda_\sigma |\sigma|^4 + \lambda_{H\sigma} |H|^2 |\sigma|^2 \\ & + \boldsymbol{\lambda}_\eta |\eta|^4 + \boldsymbol{\lambda}_\chi |\chi|^4 + \boldsymbol{\lambda}_{H\eta} |H|^2 |\eta|^2 + \boldsymbol{\lambda}'_{H\eta} |H^\dagger \eta|^2 + \boldsymbol{\lambda}_{H\chi} |H|^2 |\chi|^2 \\ & + \boldsymbol{\lambda}_{\eta\sigma} |\eta|^2 |\sigma|^2 + \boldsymbol{\lambda}_{\chi\sigma} |\chi|^2 |\sigma|^2 + \boldsymbol{\lambda}_{\eta\chi} |\eta|^2 |\chi|^2 + \left(\kappa Y_1^{(4)} \eta^\dagger H \chi + \text{h.c.} \right), \end{aligned} \quad (1)$$

where all the couplings written in the **bold** have the following definition $\boldsymbol{\Lambda} \equiv \tilde{\Lambda}/(-i\tau + i\bar{\tau})^2$ and their invariance under modular symmetry is similar to the invariance of Kähler potential [53]. The vev of the complex scalar, $\langle \sigma \rangle = v_\sigma/\sqrt{2}$, is responsible for the spontaneous breaking of the $U(1)_{\text{PQ}}$ symmetry, while the Higgs vev, $\langle H \rangle = (0, v_H/\sqrt{2})^T$, breaks the electroweak symmetry. After symmetry breaking, the mass spectrum of the scalar sector is obtained. The color neutral scalars H and σ mix with each other, whereas the colored scalars η and χ mix among themselves. The corresponding mass matrices are given below.

$$\begin{aligned} \mathcal{M}_{H\sigma}^2 &= \begin{pmatrix} 2\lambda_H v_H^2 & \lambda_{H\sigma} v_H v_\sigma \\ \lambda_{H\sigma} v_H v_\sigma & 2\lambda_\sigma v_\sigma^2 \end{pmatrix}, \\ \mathcal{M}_{\eta\chi}^2 &= \begin{pmatrix} m_\eta^2 & \kappa Y_1^{(4)} v_H/\sqrt{2} \\ \kappa Y_1^{(4)} v_H/\sqrt{2} & m_\chi^2 \end{pmatrix}, \end{aligned} \quad (2)$$

$$\text{where } m_\eta^2 \equiv \boldsymbol{\mu}_\eta^2 + \frac{1}{2} \left(\boldsymbol{\lambda}_{H\eta} + \boldsymbol{\lambda}'_{H\eta} \right) v_H^2 + \frac{1}{2} \boldsymbol{\lambda}_{\eta\sigma} v_\sigma^2 ,$$

$$m_\chi^2 \equiv \boldsymbol{\mu}_\chi^2 + \frac{1}{2} \boldsymbol{\lambda}_{H\chi} v_H^2 + \frac{1}{2} \boldsymbol{\lambda}_{\chi\sigma} v_\sigma^2 .$$

After electroweak symmetry breaking, only the electrically neutral component of η mixes with χ , while η^\pm remains unmixed. Without loss of generality, we absorb the overall phase of $\kappa Y_1^{(4)}$ by field redefinitions and take the η - χ mixing parameter to be real. The scalar fields η and χ are rotated into the mass eigenstate basis ζ_1 and ζ_2 by a rotation matrix U that diagonalizes the corresponding mass matrix, given by

$$\begin{pmatrix} \eta \\ \chi \end{pmatrix} = U \begin{pmatrix} \zeta_1 \\ \zeta_2 \end{pmatrix} = \begin{pmatrix} \cos \theta & \sin \theta \\ -\sin \theta & \cos \theta \end{pmatrix} \begin{pmatrix} \zeta_1 \\ \zeta_2 \end{pmatrix}, \quad \tan 2\theta = \frac{\sqrt{2}\kappa Y_1^{(4)} v_H}{m_\eta^2 - m_\chi^2} . \quad (3)$$

The resulting physical masses are given by,

$$m_{1,2}^2 = \frac{1}{2} \left(m_\eta^2 + m_\chi^2 \pm \sqrt{(m_\eta^2 - m_\chi^2)^2 + 2 \left(\kappa Y_1^{(4)} \right)^2 v_H^2} \right) . \quad (4)$$

Once the $U(1)_{\text{PQ}}$ and electroweak symmetries are broken, the remaining fields also acquire masses, in particular the neutrinos, as discussed next.

2.2. Leptonic Yukawa Sector and Neutrino Mass Generation

Using the charge assignments under the different symmetries shown in Table. I, the renormalizable Yukawa Lagrangian that governs the leptonic sector can be constructed as follows

$$\begin{aligned} -\mathcal{L}_y = & \alpha_\ell \left(Y_1^{(4)} \otimes \bar{L}_1 \otimes e_{R_1} \right)_1 H + \beta_\ell \left(Y_2^{(2)} \otimes \bar{L}_1 \otimes e_{R_{23}} \right)_1 H + \gamma_\ell \left(Y_2^{(4)} \otimes \bar{L}_{23} \otimes e_{R_1} \right)_1 H \\ & + \delta_\ell \left(Y_2^{(2)} \otimes \bar{L}_{23} \otimes e_{R_{23}} \right)_1 H + \alpha_\nu \left(Y_1^{(6)} \otimes \bar{L}_1 \otimes \Psi_{R_1} \right)_1 \tilde{\eta} + \beta_\nu \left(Y_{1'}^{(6)} \otimes \bar{L}_1 \otimes \Psi_{R_2} \right)_1 \tilde{\eta} \\ & + \gamma_\nu \left(Y_2^{(6)} \otimes \bar{L}_{23} \otimes \Psi_{R_1} \right)_1 \tilde{\eta} + \delta_\nu \left(Y_2^{(6)} \otimes \bar{L}_{23} \otimes \Psi_{R_2} \right)_1 \tilde{\eta} + \alpha'_\nu \left(Y_1^{(6)} \otimes \bar{\Psi}_{L_1} \otimes \nu_{R_1} \right)_1 \chi \\ & + \beta'_\nu \left(Y_2^{(4)} \otimes \bar{\Psi}_{L_1} \otimes \nu_{R_{23}} \right)_1 \chi + \gamma'_\nu \left(Y_{1'}^{(6)} \otimes \bar{\Psi}_{L_2} \otimes \nu_{R_1} \right)_1 \chi + \delta'_\nu \left(Y_2^{(4)} \otimes \bar{\Psi}_{L_2} \otimes \nu_{R_{23}} \right)_1 \chi \\ & + \alpha_\psi \left(Y_1^{(4)} \otimes \bar{\Psi}_{L_1} \otimes \Psi_{R_1} \right)_1 \sigma + \delta_\psi \left(Y_1^{(4)} \otimes \bar{\Psi}_{L_2} \otimes \Psi_{R_2} \right)_1 \sigma + \text{h.c.}, \end{aligned} \quad (5)$$

where $\tilde{\eta} \equiv i\sigma_2\eta^*$; σ_2 is the second Pauli matrix. The lower indices in parentheses 1 in the above equation denote trivial singlet representations under the S_3 symmetry. We provide the relevant modular Yukawa couplings of the model and their weights in the following Table II (see App. A for details).

		Couplings					
		$Y_{\mathbf{2}}^{(2)}$	$Y_{\mathbf{1}}^{(4)}$	$Y_{\mathbf{2}}^{(4)}$	$Y_{\mathbf{1}}^{(6)}$	$Y_{\mathbf{1}'}^{(6)}$	$Y_{\mathbf{2}}^{(6)}$
S_3	2	1	2	1	1'	2	
$-k$	2	4	4	6	6	6	

TABLE II: Modular transformation of Yukawa couplings and their weights.

The charged lepton mass matrix derived from the Lagrangian in Eq. (5) can be expressed as

$$m_\ell = \frac{v_H}{\sqrt{2}} \begin{pmatrix} \alpha_\ell Y_{\mathbf{1}}^{(4)} & \beta_\ell y_1 & \beta_\ell y_2 \\ \gamma_\ell Y_{\mathbf{2},1}^{(4)} & -\delta_\ell y_1 & \delta_\ell y_2 \\ \gamma_\ell Y_{\mathbf{2},2}^{(4)} & \delta_\ell y_2 & \delta_\ell y_1 \end{pmatrix}, \quad (6)$$

where weight 2 modular Yukawa coupling $Y_{\mathbf{2}}^{(2)} \equiv (Y_{\mathbf{2},1}^{(2)}, Y_{\mathbf{2},2}^{(2)})^T \equiv (y_1, y_2)^T$. Then, m_ℓ is diagonalized by a bi-unitary mixing matrix as $D_\ell \equiv V_{e_L}^\dagger m_\ell V_{e_R}$, therefore, $|D_\ell|^2 = V_{e_L}^\dagger m_\ell m_\ell^\dagger V_{e_L}$. We denote the mass eigenstates of vector-like fermions as Ψ_k and their masses as M_k ($k = 1, 2$), given by

$$M_1 = \alpha_\psi m_0, \quad M_2 = \delta_\psi m_0, \quad \text{where } m_0 \equiv Y_{\mathbf{1}}^{(4)} \frac{v_\sigma}{\sqrt{2}}. \quad (7)$$

The neutrino masses are generated at the one loop-level, mediated by colored fermions and scalars, as shown in Fig. 1. The resulting one loop neutrino mass matrix can be computed as follows

$$(m_\nu)_{\alpha\beta} = \frac{N_c \sin \theta \cos \theta}{16\pi^2} \sum_{k=1,2} \mathcal{Y}_{\alpha k} \mathcal{Y}'_{k\beta} M_k \left(\frac{m_1^2}{m_1^2 - M_k^2} \ln \frac{m_1^2}{M_k^2} - \frac{m_2^2}{m_2^2 - M_k^2} \ln \frac{m_2^2}{M_k^2} \right), \quad (8)$$

where N_c is the color factor, and the angle θ and masses m_1, m_2 can be followed from Eqs. (3) and (4). The fermion masses M_k are given in Eq. (7). The Yukawa structure is encoded

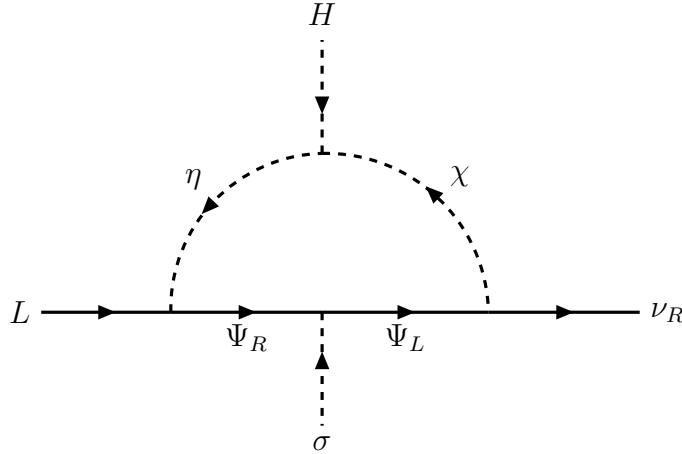


FIG. 1: One loop Dirac neutrino masses mediated by colored fields.

within the matrices \mathcal{Y} and \mathcal{Y}' , which are given by

$$\mathcal{Y} \equiv \begin{pmatrix} \alpha_\nu Y_{\mathbf{1}}^{(6)} & \beta_\nu Y_{\mathbf{1}'}^{(6)} \\ \gamma_\nu Y_{\mathbf{2},1}^{(6)} & -\delta_\nu Y_{\mathbf{2},2}^{(6)} \\ \gamma_\nu Y_{\mathbf{2},2}^{(6)} & \delta_\nu Y_{\mathbf{2},1}^{(6)} \end{pmatrix}, \quad \mathcal{Y}' \equiv \begin{pmatrix} \alpha'_\nu Y_{\mathbf{1}}^{(6)} & \beta'_\nu Y_{\mathbf{2},1}^{(4)} & \beta'_\nu Y_{\mathbf{2},2}^{(4)} \\ \gamma'_\nu Y_{\mathbf{1}'}^{(6)} & -\delta'_\nu Y_{\mathbf{2},2}^{(4)} & \delta'_\nu Y_{\mathbf{2},1}^{(4)} \end{pmatrix}. \quad (9)$$

As discussed earlier, we introduce only two generations of vector-like fermions Ψ_k . As a result, the neutrino mass matrix is of rank two, yielding masses for two neutrinos, while the lightest neutrino remains massless. This feature has important implications for the model, particularly for the sum of neutrino masses, as explored in the numerical analysis presented in the subsequent section.

In order to analyze the neutrino oscillation, we redefine m_ν to be $m_\nu \equiv \kappa_\nu \tilde{m}_\nu$, where

$$\kappa_\nu \equiv \frac{N_c \sin \theta \cos \theta}{16\pi^2} \alpha_\nu \alpha'_\nu m_0. \quad (10)$$

where $m_0 \equiv Y_{\mathbf{1}}^{(4)} \frac{v_\sigma}{\sqrt{2}}$. The neutrino mass matrix m_ν is diagonalized by a bi-unitary mixing matrix as $D_\nu \equiv V_{\nu_L}^\dagger m_\nu V_{\nu_R} = \kappa_\nu V_{\nu_L}^\dagger \tilde{m}_\nu V_{\nu_R}$, therefore, $|\tilde{D}_\nu|^2 = V_{\nu_L}^\dagger \tilde{m}_\nu \tilde{m}_\nu^\dagger V_{\nu_L}$. Then, we can rewrite κ_ν in terms of atmospheric mass-squared difference Δm_{atm}^2 and mass eigenvalues of

neutrinos as follows:

$$(\text{NH}) : \kappa_\nu^2 = \frac{\Delta m_{\text{atm}}^2}{|\tilde{D}_{\nu_3}|^2}, \quad (11)$$

$$(\text{IH}) : \kappa_\nu^2 = \frac{\Delta m_{\text{atm}}^2}{|\tilde{D}_{\nu_2}|^2}. \quad (12)$$

The solar mass-squared difference Δm_{sol}^2 is given by

$$(\text{NH}) : \Delta m_{\text{sol}}^2 = \Delta m_{\text{atm}}^2 \left(\frac{|\tilde{D}_{\nu_2}|^2}{|\tilde{D}_{\nu_3}|^2} \right), \quad (13)$$

$$(\text{IH}) : \Delta m_{\text{sol}}^2 = \Delta m_{\text{atm}}^2 \left(\frac{|\tilde{D}_{\nu_2}|^2 - |\tilde{D}_{\nu_1}|^2}{|\tilde{D}_{\nu_2}|^2} \right). \quad (14)$$

Through these relations, the neutrino mass eigenvalues are found as

$$(\text{NH}) : D_{\nu_2} = \sqrt{\Delta m_{\text{sol}}^2}, \quad D_{\nu_3} = \sqrt{\Delta m_{\text{atm}}^2}, \quad (15)$$

$$(\text{IH}) : D_{\nu_1} = \sqrt{\Delta m_{\text{atm}}^2 - \Delta m_{\text{sol}}^2}, \quad D_{\nu_2} = \sqrt{\Delta m_{\text{atm}}^2}. \quad (16)$$

The observed mixing matrix for the lepton sector is given by $U_{\text{PMNS}} \equiv V_{eL}^\dagger V_{\nu L}$. Applying the standard parametrization in PDG [102], we find three mixing angles and Dirac CP phase; δ_{CP} , to be

$$s_{13} = |U_{\text{PMNS}}|_{13}, \quad s_{12} = |U_{\text{PMNS}}|_{12}/c_{13}, \quad s_{23} = |U_{\text{PMNS}}|_{23}/c_{13}, \quad \delta_{\text{CP}} = \arg[(U_{\text{PMNS}})_{13}], \quad (17)$$

where $s_{13,12,23}$ ($c_{13,12,23}$) is abbreviation form of $\sin \theta_{13,12,23}$ ($\cos \theta_{13,12,23}$) in the three mixing angles.

3. NUMERICAL ANALYSIS AND PREDICTIONS

In this section, we present our numerical χ^2 analysis to satisfy the neutrino oscillation data as well as cLFVs and lepton $g - 2$. At first, we randomly select our input parameters

Parameter	BF	Parameter	BF	Parameter	BF
τ	$-0.0411 + 1.69i$	m_1/m_0	2.13×10^3	M_1/m_0	6.73×10^{-5}
β_ν/α_ν	2.12×10^{-4}	γ_ν/α_ν	1.27	M_2/m_0	908
β'_ν/α'_ν	0.0158	γ'_ν/α'_ν	-1.75×10^{-4}		
δ_ν/α_ν	$(-1.27 + 1.31i) \times 10^{-5}$	δ'_ν/α'_ν	$(1.75 + 6.63i) \times 10^{-4}$	m_2/m_0	2.47×10^3
β_ℓ/α_ℓ	0.993	δ_ℓ/α_ℓ	0.000365	γ_ℓ/α_ℓ	0.123
s_{12}	0.569	s_{23}	0.734	s_{13}	0.148
Δm_{sol}^2	$7.50 \times 10^{-5} \text{ eV}^2$	Δm_{atm}^2	$2.51 \times 10^{-3} \text{ eV}^2$	δ_{CP}	330°
$\sum D_\nu$	58.8 meV	$m_{\nu e}$	4.88 meV	$ \kappa_\nu ^2$	4.49×10^{-11}

TABLE III: Best-fit (BF) parameter values in the NH case corresponding to $\chi_{\min} = 2.48$.

in the following ranges:

$$[\beta_\nu^{(\prime)}/\alpha_\nu^{(\prime)}, \gamma_\nu^{(\prime)}/\alpha_\nu^{(\prime)}, \delta_\nu^{(\prime)}/\alpha_\nu^{(\prime)}] = [10^{-5}, 10^5], \quad [m_i/m_0, M_i/m_0] = [10^{-5}, 10^5], \quad (18)$$

where $m_0 \equiv Y_1^{(4)} \frac{v_\sigma}{\sqrt{2}}$, and $m_{\eta\pm} \approx m_1$ in order to simply evade constraints of oblique parameters [103]. In the scan, we additionally require perturbative couplings, a bounded from below scalar potential, and positive physical scalar masses to avoid tachyonic directions. We work on the fundamental region of τ . Then, we make use of five reliable observables provided by Nufit6.0 [104]; $[\Delta m_{\text{atm}}^2, \Delta m_{\text{sol}}^2, s_{12}^2, s_{13}^2, s_{23}^2]$, for our analysis, and we show our allowed region up to 5σ confidential level below.

3.1. Normal Hierarchy (NH)

We begin with a discussion of the NH case. From a χ^2 analysis, the best-fit (BF) values of the parameters are obtained at $\chi_{\min} = 2.48$. These values are summarized in Table III. We present our model predictions through the scattered plots. In Fig. 2, we show allowed region on $\text{Im}[\tau]$ in terms of $\text{Re}[\tau]$, where the blue points represent the range $\leq 1\sigma$, green ones ($1\sigma - 2\sigma$), yellow ones ($2\sigma - 3\sigma$), and red ones ($3\sigma - 5\sigma$)². The figure tells us that the whole range on $\text{Re}[\tau]$ is allowed, but $\text{Im}[\tau]$ is restricted by the range of [1.6-2.8]. Moreover, the allowed region is localized at $\text{Im}[\tau] \sim 1.7$. In Fig. 3, we show allowed regions on s_{12}^2 (left), s_{13}^2 (right), s_{23}^2 (bottom) in terms of the sum of neutrino masses $\sum D_\nu$ in meV unit, where the color legends of plots are the same as the case of Fig. 2. The dashed magenta vertical line is 72 meV, that is the recent combined data of DESI and CMB [105]. The horizontal

² In case of NH, we have null results within the range $\leq 1\sigma$; blue points.

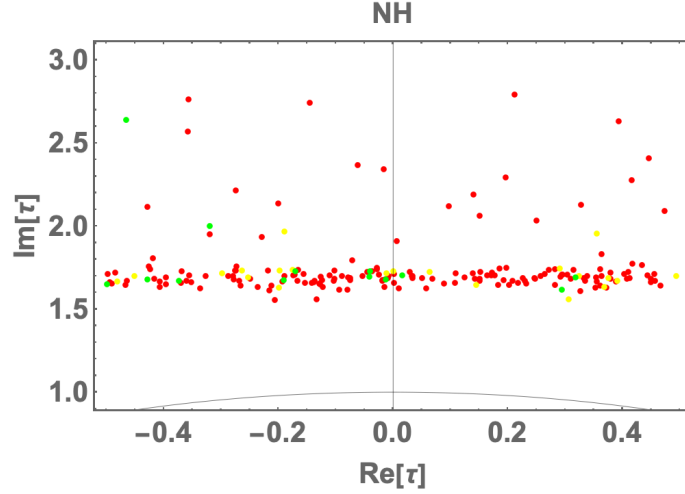


FIG. 2: Allowed region of $\text{Re}[\tau]$ and $\text{Im}[\tau]$ on the fundamental region in case of NH. Here, green points represent the range of $(1\sigma - 2\sigma)$, yellow ones $(2\sigma - 3\sigma)$, and red ones $(3\sigma - 5\sigma)$.

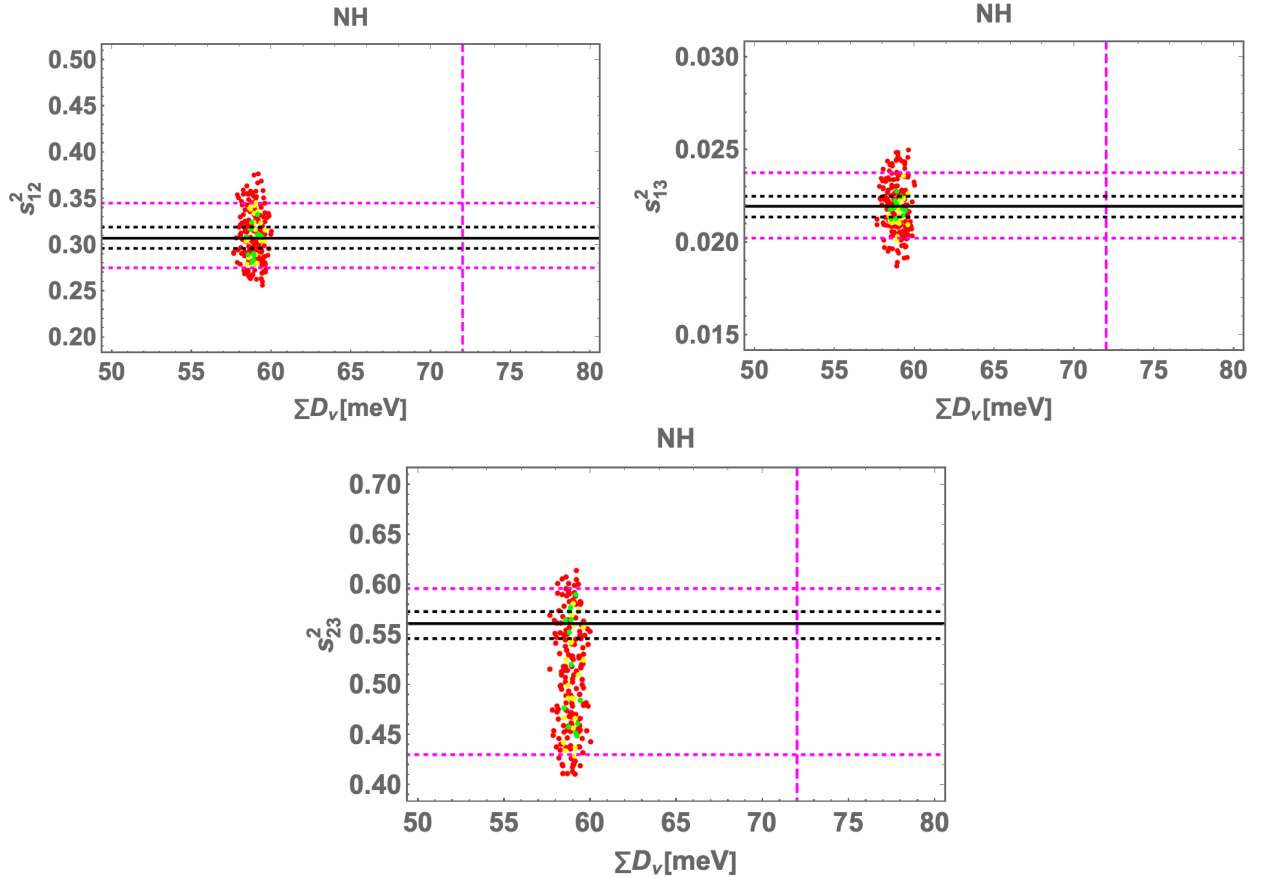


FIG. 3: Allowed regions on s_{12}^2 (left), s_{13}^2 (right), s_{23}^2 (bottom) in terms of $\sum D_\nu$, where the color legends of plots are the same as the case of Fig. 2.

lines respectively represent the best-fit value (black line), the 1σ interval (dotted black), the

3σ interval (dotted magenta), arising from two variants χ^2 analysis on Table 1 in Nufit6.0. The sum of neutrino masses, whose range is [57.6,60.0] meV, directly comes from the two experimental results of Δm_{atm}^2 and Δm_{sol}^2 , since our lightest neutrino mass eigenvalue is zero.

In Fig. 4, we demonstrate allowed regions on the Dirac CP phase δ_{CP} (left) and electron antineutrino mass m_{ν_e} (right) in terms of $\sum D_\nu$ in meV unit. The color legends of plots and vertical magenta dashed-lines are the same as the case of Fig. 3. As for the left figure,

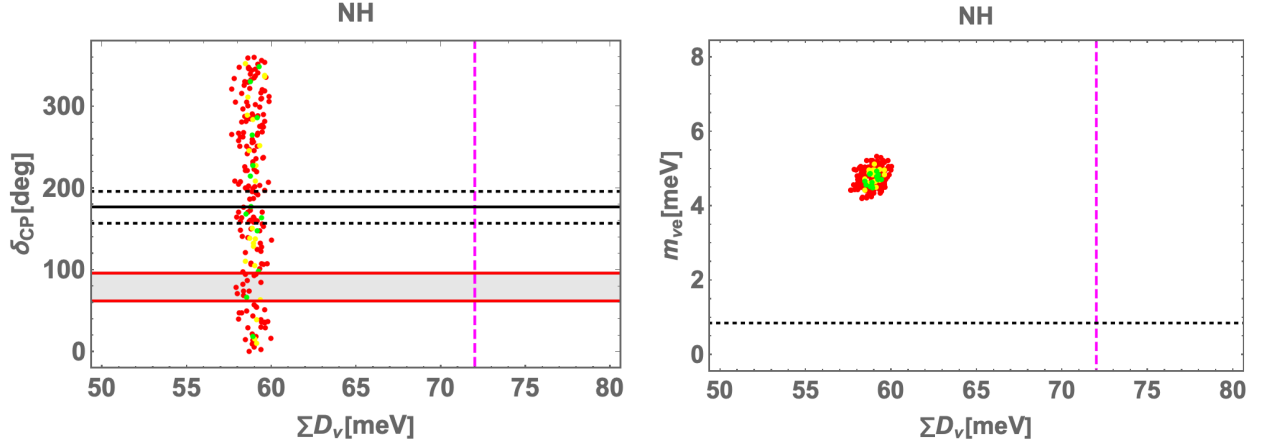


FIG. 4: Allowed regions on δ_{CP} (left) and m_{ν_e} (right) in terms of $\sum D_\nu$, where the color legends of plots are the same as the case of Fig. 3.

the horizontal black line (177 deg) is the BF value, the dotted black one (177^{+19}_{-20} deg) is the region within 1σ , and the gray region (62-96 deg) is excluded within 3σ from Nufit6.0. As for the right one, the horizontal dotted black line (0.85 meV) is the lowest upper-bound on the global analysis of oscillation data, together with the bound from the KATRIN experiment, implies that at 95% confidential level. The figure suggests that the Dirac CP phase runs over whole the region, while the effective electron antineutrino mass is localized at [4.20-5.34] meV.

3.2. Inverted Hierarchy (IH)

We now proceed to discuss the IH scenario. For this case, the BF values of the parameters are obtained at $\chi_{\text{min}} = 1.88$ and summarized in Table IV. In Fig. 5, we show the allowed region on $\text{Im}[\tau]$ in terms of $\text{Re}[\tau]$, where the color legends of plots are the same as the one in Fig. 2. The figure tells us that $\text{Re}[\tau]$ and $\text{Im}[\tau]$ are respectively localized at $[-0.156, 0.147]$ and $[1.63, 1.74]$. In Fig. 6, we show allowed regions on s_{12}^2 (left), s_{13}^2 (right), s_{23}^2 (bottom)

Parameter	BF	Parameter	BF	Parameter	BF
τ	$-0.0332 + 1.70i$	m_1/m_0	6.01×10^3	M_1/m_0	1.59×10^3
β_ν/α_ν	-2.39×10^{-2}	γ_ν/α_ν	-0.790	M_2/m_0	122
β'_ν/α'_ν	-169	γ'_ν/α'_ν	35.5		
δ_ν/α_ν	$0.733 + 0.492i$	δ'_ν/α'_ν	$(1.48 + 2.24i) \times 10^3$	m_2/m_0	5.89×10^3
β_ℓ/α_ℓ	0.994	δ_ℓ/α_ℓ	0.000365	γ_ℓ/α_ℓ	0.123
s_{12}	0.538	s_{23}	0.742	s_{13}	0.149
Δm_{sol}^2	$7.47 \times 10^{-5} \text{ eV}^2$	Δm_{atm}^2	$2.49 \times 10^{-3} \text{ eV}^2$	δ_{CP}	332°
$\sum D_\nu$	99.1 meV	$m_{\nu e}$	48.9 meV	$ \kappa_\nu ^2$	3.04×10^{-28}

TABLE IV: Best-fit (BF) parameter values in the IH case corresponding to $\chi_{\min} = 1.88$.

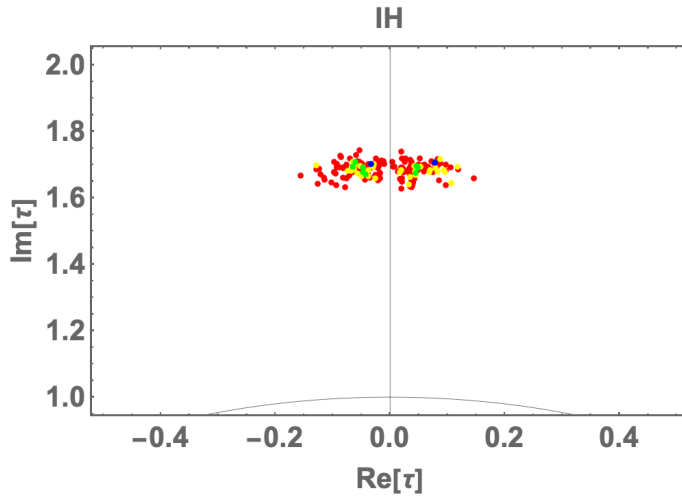


FIG. 5: Allowed region on $\text{Im}[\tau]$ in terms of $\text{Re}[\tau]$, where the color legends of plots are the same as the one in Fig. 2.

in terms of $\sum D_\nu$ in meV unit, where the color legends of plots and lines are the same as the case of Fig. 3. The magenta vertical dotted line at 120 meV is the upper bound by the minimal standard cosmological model with CMB data [6]. The sum of neutrino masses, whose range is [97.5,101] meV, directly comes from the two experimental results of Δm_{atm}^2 and Δm_{sol}^2 , since our lightest neutrino mass eigenvalue is zero.

In Fig. 7, we demonstrate allowed regions on δ_{CP} (left) and $m_{\nu e}$ (right) in terms of $\sum D_\nu$, where the color legends of plots and vertical magenta dashed-lines are the same as the case of Fig. 4. As for the left figure, the horizontal black line (285 deg) is the BF value, the dotted black one (285^{+25}_{-28} deg) is the region within 1σ , and the gray region ([0, 201] deg and [348, 360] deg) is excluded within 3σ from Nufit6.0. As for the right one, the horizontal dotted black line (48 meV) is the lowest upper-bound on the global analysis of oscillation data, together with the bound from the KATRIN experiment, implies that at 95% confidential level. The

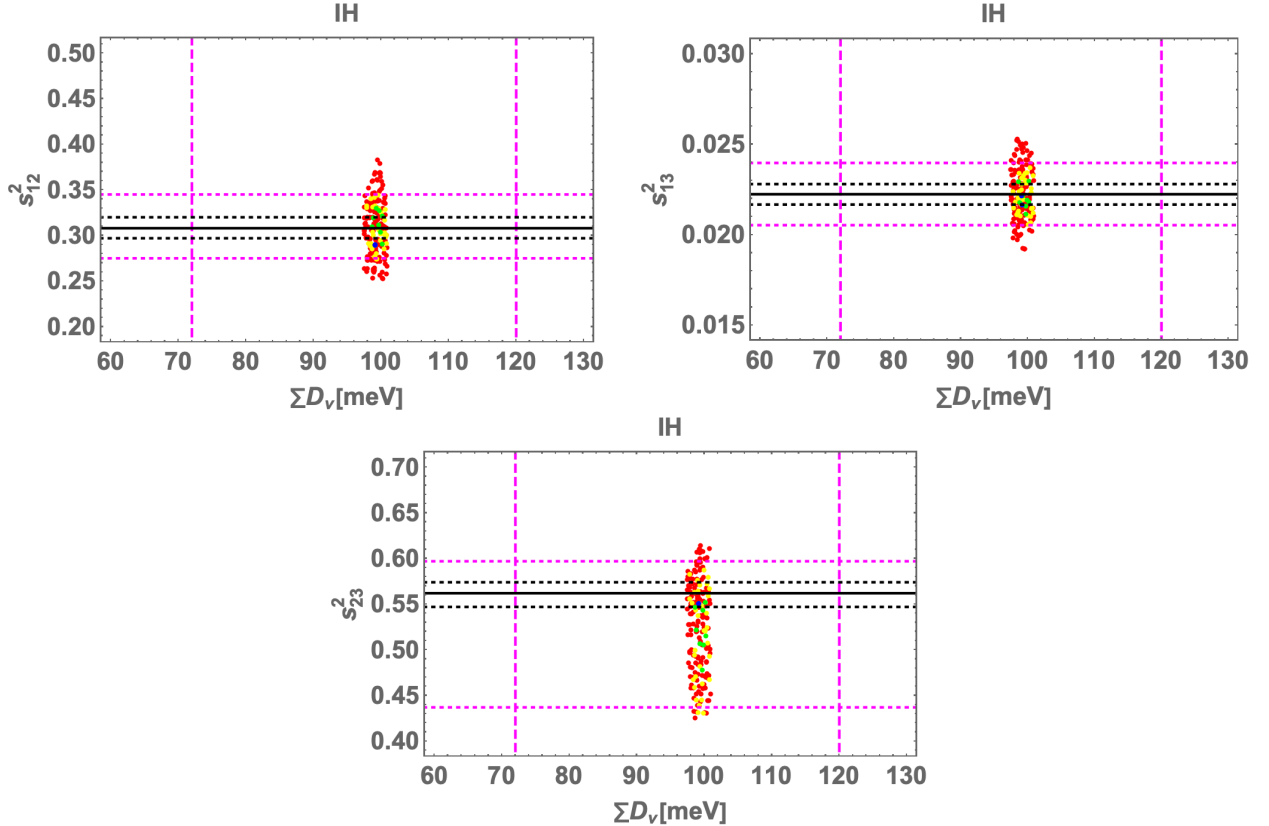


FIG. 6: Allowed regions on s_{12}^2 (left), s_{13}^2 (right), s_{23}^2 (bottom) in terms of $\sum D_\nu$, where the color legends are the same as the case of Fig. 3.

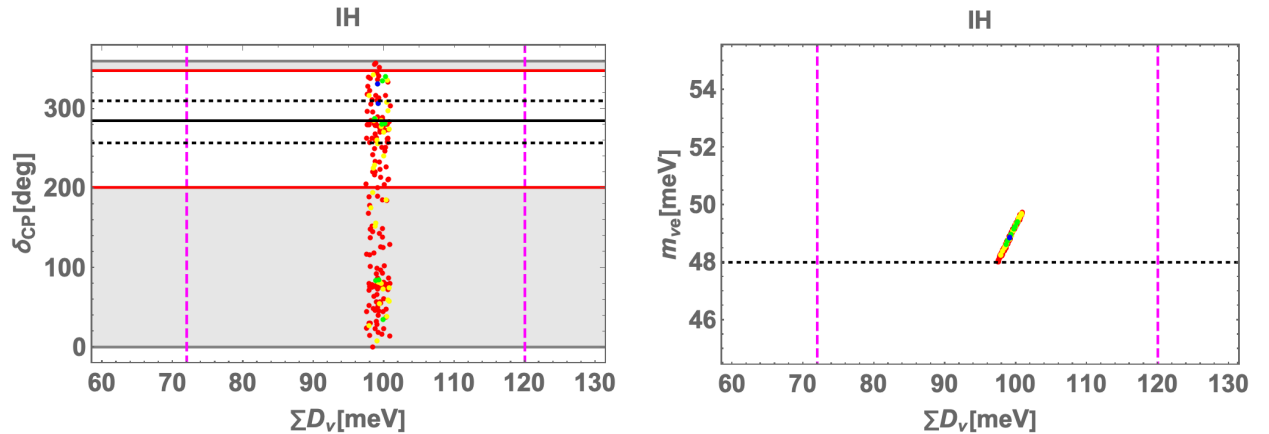


FIG. 7: Allowed regions on δ_{CP} (left) and m_{ν_e} (right) in terms of $\sum D_\nu$, where the color legends of plots and vertical magenta dashed-lines are the same as the case of Fig. 4.

figure suggests us that the Dirac CP phase runs over whole the region, while the effective electron antineutrino mass is localized at [48.0-49.7] meV. This region is interestingly located at nearby 48 meV that is the lowest upper-bound on the global analysis.

4. CHARGED LEPTON FLAVOR VIOLATION (cLFV) AND LEPTON $g-2$

Extensions of the SM that account for neutrino mass generation, particularly low scale constructions [106–109], are often accompanied by sizable charged lepton flavor violating (cLFV) processes as well. This has led to an extensive experimental efforts [110–119] dedicated to probing rare cLFV processes, particularly muon and tau decays. In our model, cLFV processes are induced by the Yukawa interactions $\bar{L}_\alpha \Psi_{R_j} \tilde{\eta}$, and the corresponding interaction Lagrangian can be written as

$$\mathcal{L} \supset \alpha_\nu Y_{\mathbf{1}}^{(6)} \bar{e} \Psi_{R_1} \tilde{\eta} + \gamma_\nu \left(Y_{\mathbf{2},1}^{(6)} \bar{\mu} + Y_{\mathbf{2},2}^{(6)} \bar{\tau} \right) \Psi_{R_1} \tilde{\eta} \\ + \beta_\nu Y_{\mathbf{1}'}^{(6)} \bar{e} \Psi_{R_2} \tilde{\eta} + \delta_\nu \left(Y_{\mathbf{2},1}^{(6)} \bar{\tau} - Y_{\mathbf{2},2}^{(6)} \bar{\mu} \right) \Psi_{R_2} \tilde{\eta}. \quad (19)$$

We consider the cLFV processes $\ell_\alpha \rightarrow \ell_\beta \gamma$ ($\equiv (\mu \rightarrow e\gamma)$, $(\tau \rightarrow e\gamma)$, $(\tau \rightarrow \mu\gamma)$) as shown in

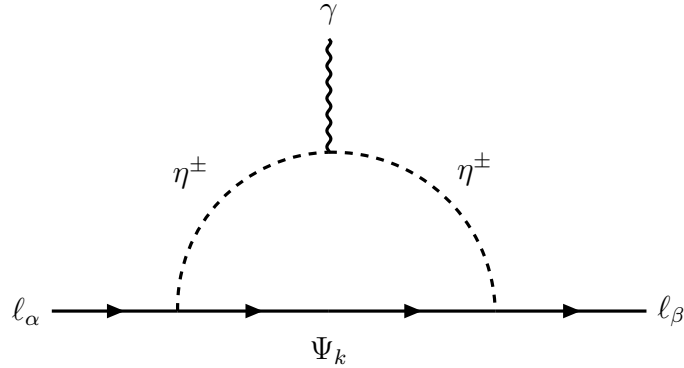


FIG. 8: One loop Feynman diagram for the cLFV processes $\ell_\alpha \rightarrow \ell_\beta \gamma$.

Fig. 8, and the corresponding branching ratio (\mathcal{BR}) is given by

$$\mathcal{BR}(\ell_\alpha \rightarrow \ell_\beta \gamma) \approx \mathcal{BR}(\ell_\alpha \rightarrow \ell_\beta \nu_\alpha \bar{\nu}_\beta) \times \frac{3\alpha_e N_c}{16\pi G_F^2} \left| \sum_{k=1}^2 \mathcal{Y}_{\beta k} \mathcal{Y}_{k\alpha}^\dagger \mathcal{F}(M_{\Psi_k}, m_{\eta^\pm}) \right|^2, \quad (20)$$

$$\mathcal{F}(x, y) \approx \frac{2x^6 + 3x^4y^2 - 6x^2y^4 + y^6 - 12x^4y^2 \ln\left(\frac{x}{y}\right)}{12(x^2 - y^2)^4}, \quad (21)$$

$$\mathcal{BR}(\mu \rightarrow e \nu_\mu \bar{\nu}_e) \approx 1, \quad \mathcal{BR}(\tau \rightarrow e \nu_\tau \bar{\nu}_e) \approx 0.1785, \quad \mathcal{BR}(\tau \rightarrow \mu \nu_\tau \bar{\nu}_\mu) \approx 0.1737. \quad (22)$$

Here, $\alpha_e \approx 1/137$ is the fine structure constant, N_c is color factor, Fermi constant $G_F = 1.166 \times 10^{-5}$ GeV $^{-2}$, and the matrix of Yukawa couplings \mathcal{Y} is provided in Eq. (9). The

current stringent experimental upper bounds for the branching ratios of the $\ell_\alpha \rightarrow \ell_\beta \gamma$ processes are given by [113, 116, 120]

$$\mathcal{BR}(\mu \rightarrow e\gamma) \lesssim 3.10 \times 10^{-13}, \quad \mathcal{BR}(\tau \rightarrow e\gamma) \lesssim 3.30 \times 10^{-8}, \quad \mathcal{BR}(\tau \rightarrow \mu\gamma) \lesssim 4.20 \times 10^{-8}. \quad (23)$$

Following the Eq. (20), and the BF values of our numerical analysis provided in Table III (Table IV) for NH (IH) case, the branching ratios for $\mathcal{BR}(\ell_\alpha \rightarrow \ell_\beta \gamma)$ in our model can be calculated as follows

$$\text{NH : } \mathcal{BR}(\mu \rightarrow e\gamma) \lesssim 3.10 \times 10^{-13}, \quad \mathcal{BR}(\tau \rightarrow e\gamma) \lesssim 1.54 \times 10^{-8}, \quad \mathcal{BR}(\tau \rightarrow \mu\gamma) \lesssim 2.07 \times 10^{-13}, \quad (24)$$

$$\text{IH : } \mathcal{BR}(\mu \rightarrow e\gamma) \lesssim 3.10 \times 10^{-13}, \quad \mathcal{BR}(\tau \rightarrow e\gamma) \lesssim 2.76 \times 10^{-11}, \quad \mathcal{BR}(\tau \rightarrow \mu\gamma) \lesssim 4.15 \times 10^{-8}. \quad (25)$$

Analogous to the cLFV processes discussed above, the muon and electron $g - 2$ receive loop-induced contributions in the present model. These contributions can be expressed as

$$\Delta a_\ell \approx -\frac{m_\ell^2 N_c}{16\pi^2} \sum_{k=1}^2 \mathcal{Y}_{\ell k} \mathcal{Y}_{k\ell}^\dagger \mathcal{F}(M_{\Psi_k}, m_{\eta^\pm}), \quad (26)$$

where $\ell = e, \mu$. Following the BF values of our numerical analysis, we get the following results for the lepton $g - 2$:

$$\text{NH : } |\Delta a_e| \lesssim 7.88 \times 10^{-16}, \quad |\Delta a_\mu| \lesssim 1.59 \times 10^{-13}, \quad (27)$$

$$\text{IH : } |\Delta a_e| \lesssim 2.21 \times 10^{-18}, \quad |\Delta a_\mu| \lesssim 2.37 \times 10^{-12}. \quad (28)$$

Here, we can always fix the maximum value for $\mathcal{BR}(\mu \rightarrow e\gamma)$ to be 3.10×10^{-13} , which is the experimental upper limit, since we have enough parameters. Then, the other cLFVs as well as lepton $g - 2$ are predicted by our model. In addition to good verifiability of $\mathcal{BR}(\mu \rightarrow e\gamma)$, $\mathcal{BR}(\tau \rightarrow e\gamma)$ for NH can be a verifiable process, while $\mathcal{BR}(\tau \rightarrow \mu\gamma)$ for IH can be a verifiable one.

5. AXION AND ITS ROLE AS DARK MATTER

We now delve into a detailed discussion of axion and its potential role as a DM candidate. The complex scalar σ can be parameterized as $\sigma = (v_\sigma + \rho) \exp(ia/v_\sigma)/\sqrt{2}$, where a corresponds to the axion and ρ is the radial mode. Once the scalar σ acquires a vev, the PQ symmetry is spontaneously broken at a scale $f_{\text{PQ}} \equiv \langle \sigma \rangle = v_\sigma/\sqrt{2}$. The axion decay constant f_a is directly related to the PQ breaking scale f_{PQ} , which is given by

$$f_a = \frac{f_{\text{PQ}}}{N} = \frac{v_\sigma}{\sqrt{2}N} , \quad (29)$$

where N denotes the color anomaly factor. A nonzero color anomaly factor N is essential for the axion to couple to gluons and thereby provide a consistent solution to the strong CP problem. For our model the N is given as follows (ω is PQ charge of Ψ),

$$\begin{aligned} N &= 2 \sum_f \left(\omega_L^f - \omega_R^f \right) T(R_f) \\ &= 2(q + \frac{1}{2} - q + q + \frac{1}{2} - q) T(1, 0) \\ &= 1, \quad T(1, 0) \equiv \frac{1}{2}. \end{aligned} \quad (30)$$

This value of the color anomaly factor remains consistent with the original KSVZ axion models [43, 44]. The QCD axion mass, obtained from the non-perturbative potential at next-to-leading order (NLO), is given as follows [121],

$$m_a = 5.70(7) \left(\frac{10^{12} \text{GeV}}{f_a} \right) \mu\text{eV}. \quad (31)$$

This relation between m_a and f_a is a model independent prediction of the QCD axion, provided that the PQ symmetry is explicitly broken only by non-perturbative QCD effects. In the following subsection, we discuss how the f_a is determined from DM relic density constraints, which in turn predicts the value of m_a .

5.1. Axion Dark Matter

In addition to resolving the strong CP problem, the axion is an attractive DM candidate: it is light, very weakly interacting, and stable on cosmological timescales. In the early

Universe, axions are typically produced non-thermally, yielding a cold DM component. A substantial fraction of the axion DM abundance can be generated via the misalignment mechanism [50–52], which is given by [122]

$$\Omega_{a,\text{mis}} h^2 \simeq \Omega_{\text{CDM}} h^2 \langle \theta_0^2 \rangle \left(\frac{f_a}{2 \times 10^{11} \text{ GeV}} \right)^{7/6}, \quad (32)$$

where θ_0 denotes the initial misalignment angle and $\langle \theta_0^2 \rangle$ depends on whether the PQ symmetry is broken before or after inflation.

If the PQ symmetry is broken after inflation, the initial misalignment angle θ_0 varies randomly between causally disconnected patches, and one averages over θ_0 with the periodic axion potential (including anharmonicities), giving $\langle \theta_0^2 \rangle \sim 2.15^2$ [122, 123]. Assuming that axions produced via misalignment account for the entire cold DM abundance, Eq. (32) yields $f_a \simeq 5.4 \times 10^{10}$ GeV, leading to $m_a \simeq 106$ μeV via Eq. (31).

Moreover, the formation and decay of cosmic strings and domain walls can substantially enhance the axion relic abundance in the post-inflationary scenario. Accounting for these contributions, the total relic density is given by [124]

$$\Omega_{a,\text{tot}} h^2 \simeq (1.6 \pm 0.4) \times 10^{-2} \left(\frac{f_a}{10^{10} \text{ GeV}} \right)^{(6+n)/(4+n)}, \quad (33)$$

with the QCD scale fixed at 400 MeV and $n = 6.68$. Consequently, one finds

$$\Omega_{a,\text{tot}} h^2 \simeq 3 \Omega_{a,\text{mis}} h^2. \quad (34)$$

These additional contributions effectively shift the value of f_a required to reproduce the observed DM abundance, and thus imply a correspondingly shifted axion mass range. Requiring that $\Omega_{a,\text{tot}} h^2$ accounts for 100% of cold DM, we obtain

$$f_a \simeq (4.5 - 7.0) \times 10^{10} \text{ GeV}, \quad m_a \simeq (81 - 127) \text{ } \mu\text{eV}. \quad (35)$$

In the remainder of this section (and in Sec. 5.2 below), we will use Eq. (35) as a concrete post-inflationary benchmark to present definite numerical expectations for axion searches.

If instead the PQ symmetry is broken before (or during) inflation and is not restored afterwards, inflation homogenizes the axion field over our observable Universe, so θ_0 is effec-

tively a single constant value rather than a random variable. In this case, topological defects are inflated away in our observable patch, and one should replace $\langle \theta_0^2 \rangle \rightarrow \theta_0^2$ in Eq. (32). As a result, the DM motivated f_a (and thus m_a) becomes θ_0 -dependent, and the axion parameter space is naturally described as a band rather than a single narrow interval. This pre-inflationary setup can also lead to observable imprints via primordial axion fluctuations, reflected in CMB anisotropies and large-scale structure; these effects are subject to isocurvature constraints (model and inflation scale dependent), which we do not analyze further here.

The present model contains colored exotic scalars and vector-like colored fermions, and depending on the mass ordering, the lightest colored exotic can be stable (or long-lived) at the renormalizable level. For the best-fit points in Tables III and IV, the colored scalar mass eigenstates are heavier than at least one colored fermion, so the scalars can decay into Ψ plus leptons/ ν_R through the Yukawa interactions in Eq. (5). However, this does not by itself guarantee the absence of stable colored relics, since the lightest colored fermion may remain stable in the minimal setup. Therefore, if a post-inflationary thermal history is assumed, one would generally need either (i) additional allowed interactions/operators that ensure sufficiently fast decays of the lightest colored state, or (ii) a sufficiently low reheating history so that the colored sector is not regenerated after inflation. In contrast, the pre-inflationary PQ breaking cosmology provides a simple, consistent setting in which any primordial abundance is diluted by inflation and the colored sector is not repopulated, provided the maximum temperature after inflation remains below the lightest colored mass scale, and non-thermal production is negligible.

Finally, while the standard misalignment mechanism [50–52] has long been regarded as the primary source of axion DM, recent developments have highlighted the kinetic misalignment mechanism [125], where the initial axion velocity \dot{a}_0 (or kinetic energy) can play a crucial role. In this scenario, the axion field evolves from initial conditions defined by a nonzero \dot{a}_0 and a misalignment angle θ_0 . Once the axion field begins coherent oscillations, it behaves as cold DM, and its relic density can be estimated accordingly. If the kinetic energy density exceeds the axion potential barrier at a given temperature, the onset of oscillations is delayed until the kinetic energy becomes subdominant, potentially modifying the final relic abundance.

5.2. Axion-Photon Coupling

The axion experimental program spans a variety of complementary detection strategies, with helioscopes and haloscopes serving as key probes. Together with indirect constraints from astrophysical and cosmological observations, axions are typically probed primarily through the axion-photon coupling. This coupling arises in the effective Lagrangian

$$\mathcal{L} = \frac{g_{a\gamma\gamma}}{4} a F_{\mu\nu} \tilde{F}^{\mu\nu}, \quad (36)$$

where $g_{a\gamma\gamma}$ denotes the axion-photon coupling, $F_{\mu\nu}$ is the electromagnetic field strength, and $\tilde{F}^{\mu\nu}$ is its dual. Utilizing NLO chiral Lagrangian techniques [121], the axion-photon coupling is given by

$$g_{a\gamma\gamma} = \frac{\alpha_e}{2\pi f_a} \left[\frac{E}{N} - 1.92(4) \right]. \quad (37)$$

Within our model framework, since the only chiral fermions with nonvanishing PQ charges are the $SU(2)_L$ singlet fields Ψ_i , the ratio of the electromagnetic and color anomaly factors is $E/N = 0$. Thus Eq. (37) simplifies to

$$g_{a\gamma\gamma} = -1.92(4) \frac{\alpha_e}{2\pi f_a}. \quad (38)$$

Using the post-inflationary relic density motivated range of f_a in Eq. (35), our model predicts

$$|g_{a\gamma\gamma}| \simeq (3 - 5) \times 10^{-14} \text{ GeV}^{-1},$$

corresponding to $m_a \simeq (81 - 127) \text{ }\mu\text{eV}$. This provides a definite target region for the axion searches in the post-inflationary cosmological history discussed in Sec. 5.1.

In the pre-inflationary scenario, Eq. (38) remains valid, but f_a is determined by the (unknown) single value of θ_0 in our Hubble patch through Eq. (32). Therefore, the model predicts a continuous band in the $(m_a, g_{a\gamma\gamma})$ plane rather than a narrow interval. In this sense, Eq. (35) should be viewed as a concrete post-inflationary benchmark, while the pre-inflationary case maps to a broader θ_0 -dependent region.

Upcoming helioscope and haloscope searches, including IAXO [126], ADMX [127], MADMAX [128], and CAPP [129], will significantly extend the sensitivity to unexplored re-

gions of axion parameter space, probing smaller values of $|g_{a\gamma\gamma}|$ over a broad range of axion masses m_a and strengthening constraints on axion DM models. The IAXO experiment is expected to probe the $|g_{a\gamma\gamma}|$ down to $(10^{-12} - 10^{-11}) \text{ GeV}^{-1}$. Similarly, the mass regions $1 \mu\text{eV} \lesssim m_a \lesssim 100 \mu\text{eV}$ and $50 \mu\text{eV} \lesssim m_a \lesssim 120 \mu\text{eV}$ will be probed at ADMX and MAD-MAX, respectively. Moreover, CAPP is expected to probe $|g_{a\gamma\gamma}|$ down to $10^{-16} \text{ GeV}^{-1}$, with a focus on the mass region $(1 - 10) \mu\text{eV}$, extending their search to higher mass up to $30 \mu\text{eV}$ as well. Therefore, the predicted ranges of $g_{a\gamma\gamma}$ and m_a in our model lie well within the sensitivity of forthcoming experiments, offering a promising opportunity for experimental probe in the near future.

Indirect probes of axion DM models arise from astrophysical and cosmological observations, where axion DM may decay or convert into photons in regions with intense magnetic fields or high matter densities [122, 130]. Such indirect probes span a wide range of axion masses, from the ultralight regime ($m_a \lesssim 10^{-14} \text{ eV}$) to masses well above the MeV scale. Our current model framework, lies in the mass region $m_a \sim \mathcal{O}(10 - 100) \mu\text{eV}$. The Breakthrough Listen project, using radio surveys in the C-band have searched for axion to photon conversion in magnetospheres of neutron stars near the Galactic Center. These searches place upper limits on the axion-photon coupling $g_{a\gamma\gamma} \lesssim 10^{-11} \text{ GeV}^{-1}$ for axion masses in the range $15 \mu\text{eV} \lesssim m_a \lesssim 35 \mu\text{eV}$ [131]. Likewise, the analyses of radio data obtained from the Bullet Cluster (1E 0657-55.8) observations constraints the $g_{a\gamma\gamma} \sim (10^{-12} - 10^{-11}) \text{ GeV}^{-1}$ for $10 \mu\text{eV} \lesssim m_a \lesssim 30 \mu\text{eV}$ [132]. The presence of axions can significantly modify stellar evolution by enhancing cooling processes, such as the Primakoff effect. In particular, observations of horizontal branch stars in globular clusters impose a strong upper limit of $g_{a\gamma\gamma} \lesssim 6.6 \times 10^{-11} \text{ GeV}^{-1}$ [133]. This is consistent with limits obtained from the CAST helioscope, which places comparable limits on $g_{a\gamma\gamma}$ for $m_a \lesssim 0.02 \text{ eV}$ [134]. Furthermore, updated limits from SN 1987A gamma ray observations have tightened constraints on the $g_{a\gamma\gamma}$ by including axion to photon conversion in the magnetic field of the supernova progenitor itself, yielding $g_{a\gamma\gamma} \lesssim 10^{-11} \text{ GeV}^{-1}$ for axion mass in the range $1 \mu\text{eV} \lesssim m_a \lesssim 10^3 \mu\text{eV}$ [135]. These results correspond to an order of magnitude improvement over earlier bounds, which relied solely on axion to photon conversion in the Galactic magnetic field. In our model, the predicted axion-photon coupling lies well below current experimental and astrophysical bounds, ensuring consistency with all existing constraints.

6. CONCLUSIONS

In this work, we have presented a unified axion model framework where tiny neutrino masses, the leptonic flavor structure, the strong CP problem, and dark matter can be explained utilizing a global $U(1)_{\text{PQ}}$ and modular S_3 symmetry. This framework is implemented in a novel class of KSVZ-type axion models, where exotic colored fermions and scalars simultaneously serve as mediators for neutrino mass generation at the one loop-level. The PQ charge assignment serves multiple purposes: it forbids neutrino masses at the tree-level, and its spontaneous breaking to a residual Z_3 symmetry further ensures the Dirac nature of neutrinos. A SM singlet complex scalar σ has been introduced, whose vev is responsible for the breaking of $U(1)_{\text{PQ}}$ and leads to the emergence of the axion as a pseudo-Goldstone boson. For the minimal realization of the model, we include only two generations of the colored fermion Ψ mediating the loop. As a result, the neutrino mass matrix is of rank two, yielding masses for two neutrinos while leaving one neutrino massless.

Our numerical analysis shows that the model successfully accommodates both NH and IH of neutrino masses, while remaining consistent with experimental observations. We perform a χ^2 analysis to fit the neutrino oscillation data. In the NH scenario, no parameter points are found within the 1σ region. The entire range of $\text{Re}[\tau]$ is allowed, while $\text{Im}[\tau]$ is localized near 1.7. In contrast, for IH, both $\text{Re}[\tau]$ and $\text{Im}[\tau]$ are confined to narrow intervals, $\text{Re}[\tau] \in [-0.156, 0.147]$ and $\text{Im}[\tau] \in [1.63, 1.74]$. With the lightest neutrino mass to be zero, the sum of neutrino masses, $\sum D_\nu$ is directly intertwined with the Δm_{atm}^2 and Δm_{sol}^2 . Consequently, we obtain $\sum D_\nu \simeq 58$ (100) meV for the NH (IH), consistent with current cosmological bounds from the combined DESI and CMB data. We present model correlations of mixing angles, Dirac CP phase (δ_{CP}), and effective mass (m_{ν_e}) with the $\sum D_\nu$. Moreover, m_{ν_e} is constrained to a narrow range, with $m_{\nu_e} \simeq 5$ (49) meV for NH (IH). In particular, m_{ν_e} exhibits a robust correlation with $\sum D_\nu$ and is located near the lowest upper-bound on the global analysis for IH scenario. We provide the best-fit parameter values in the NH (IH) case corresponding to $\chi_{\text{min}} = 2.48$ (1.88) in Table III (Table IV). Using the best-fit parameter values, we analyze the cLFV rates and the lepton $g - 2$, which remain consistent with the experimental data.

Furthermore, the axion emerging from our model framework simultaneously addresses the strong CP problem and constitutes a viable DM candidate across multiple cosmological

scenarios, including post-inflationary string induced contributions and kinetic misalignment production. Requiring the axion to account for the observed DM abundance determines its decay constant and mass, which in turn predict an axion-photon coupling in the range $|g_{a\gamma\gamma}| \simeq (3 - 5) \times 10^{-14} \text{ GeV}^{-1}$. This range lies within the sensitivity of the next-generation axion searches. Notably, the resulting predictions are fully compatible with current astrophysical and cosmological limits. In summary, our explicit model presents a predictive and experimentally accessible explanation of neutrino masses, the strong CP problem, and dark matter, unifying axion phenomenology with leptonic flavor structure via an underlying modular symmetry.

ACKNOWLEDGMENTS

SKK and RK are supported by the National Research Foundation of Korea under grant NRF-2023R1A2C100609111. HO is supported by Zhongyuan Talent (Talent Recruitment Series) Foreign Experts Project.

Appendix A: S_3 tensor product rules and modular Yukawa construction

1. S_3 symmetry and its tensor product

The set of all possible permutations of three objects is described by the symmetric group S_3 . It has $3! = 6$ elements and the generators of this group are given by [53–55],

$$\rho(S) = \begin{pmatrix} 1 & 0 \\ 0 & -1 \end{pmatrix}, \quad \rho(T) = \frac{1}{2} \begin{pmatrix} -1 & -\sqrt{3} \\ -\sqrt{3} & 1 \end{pmatrix}, \quad (\text{A1})$$

which obey the following relations

$$(\rho(S))^2 = (\rho(T))^2 = (\rho(S)\rho(T))^3 = \mathbb{I}. \quad (\text{A2})$$

The group has 3 irreducible representations, a trivial singlet 1, a non-trivial singlet 1', and a doublet 2. The product rules are given as follows

$$1' \otimes 1' = 1, \quad 1' \otimes 2 = 2, \quad 2 \otimes 2 = 1 \oplus 1' \oplus 2. \quad (\text{A3})$$

Given two singlets x, y and two doublets $a = (a_1, a_2)^T, b = (b_1, b_2)^T$, their tensor product rules following Eq. (A3) can be expressed as follows [53–55]

$$\begin{aligned} (x)_{1'} \otimes (y)_{1'} &= (xy)_1, \quad (x)_{1'} \otimes \begin{pmatrix} a_1 \\ a_2 \end{pmatrix}_2 = \begin{pmatrix} -xa_2 \\ xa_1 \end{pmatrix}_2 \\ \begin{pmatrix} a_1 \\ a_2 \end{pmatrix}_2 \otimes \begin{pmatrix} b_1 \\ b_2 \end{pmatrix}_2 &= (a_1 b_1 + a_2 b_2)_1 \oplus (a_1 b_2 - a_2 b_1)_{1'} \oplus \begin{pmatrix} -a_1 b_1 + a_2 b_2 \\ a_1 b_2 + a_2 b_1 \end{pmatrix}_2. \end{aligned} \quad (\text{A4})$$

2. Modular Yukawa based on S_3

Here, we provide the discussion of modular Yukawa construction in the context of S_3 symmetry. The modular group $\bar{\Gamma}$ attains a linear fractional transformation γ , acting on the modulus τ in the upper-half complex plane. The transformation is defined as follows

$$\tau \longrightarrow \gamma\tau = \frac{a\tau + b}{c\tau + d}, \quad \text{where } a, b, c, d \in \mathbb{Z}, \quad \text{and } ad - bc = 1, \quad \text{Im}[\tau] > 0. \quad (\text{A5})$$

This is isomorphic to the transformation $PSL(2, \mathbb{Z}) = SL(2, \mathbb{Z})/\{I, -I\}$. The modular transformation is generated by two fundamental operations, S and T given by

$$S : \tau \longrightarrow -\frac{1}{\tau}, \quad T : \tau \longrightarrow \tau + 1, \quad (\text{A6})$$

These operations satisfy the algebraic relations, $S^2 = \mathbb{I}$, and $(ST)^3 = \mathbb{I}$. We consider a series of groups, denoted as $\Gamma(N)$ for $N = 1, 2, 3, \dots$, defined as follows

$$\Gamma(N) = \left\{ \begin{pmatrix} a & b \\ c & d \end{pmatrix} \in SL(2, \mathbb{Z}) \mid \begin{pmatrix} a & b \\ c & d \end{pmatrix} \equiv \begin{pmatrix} 1 & 0 \\ 0 & 1 \end{pmatrix} \pmod{N} \right\}. \quad (\text{A7})$$

For $N = 2$, we denote $\bar{\Gamma}(2) \equiv \Gamma(2)/\{I, -I\}$. Since the element $-I$ is not in $\Gamma(N)$ for $N > 2$, one can have $\bar{\Gamma}(N) = \Gamma(N)$, which are infinite normal subgroups of $\bar{\Gamma}$, referred to as

principal congruence subgroups. The quotient groups, defined as $\Gamma_N \equiv \bar{\Gamma}/\bar{\Gamma}(N)$, come from finite modular groups. For these finite groups, the condition $T^N = \mathbb{I}$ is imposed. Specifically, the groups Γ_N with $N = 2, 3, 4, 5$ are isomorphic to S_3 , A_4 , S_4 , and A_5 , respectively [136]. Modular forms of level N are holomorphic functions $f(\tau)$, which transform under the action of $\Gamma(N)$ as

$$f(\gamma\tau) = (c\tau + d)^{k_I} f(\tau) , \quad \gamma \in \Gamma(N) , \quad (\text{A8})$$

where $k_I \geq 0$ is referred to as the modular weight. For $k_I = 0$, the modular form is a constant. In this work, we discussed the group S_3 , which corresponds to $N = 2$.

The group S_3 exhibits three irreducible representations: a trivial singlet 1, a non-trivial singlet $1'$, and a doublet 2. The lowest modular weight is 2 and the corresponding modular coupling is represented as $Y_2^{(2)} \equiv (Y_{2,1}^{(2)}(\tau), Y_{2,2}^{(2)}(\tau))^T \equiv (y_1(\tau), y_2(\tau))^T$. In terms of Dedekind eta-function $\eta(\tau)$, it can be expressed as [54]

$$\begin{aligned} y_1(\tau) &= \frac{i}{4\pi} \left(\frac{\eta'(\tau/2)}{\eta(\tau/2)} + \frac{\eta'((\tau+1)/2)}{\eta((\tau+1)/2)} - \frac{8\eta'(2\tau)}{\eta(2\tau)} \right) , \\ y_2(\tau) &= \frac{\sqrt{3}i}{4\pi} \left(\frac{\eta'(\tau/2)}{\eta(\tau/2)} - \frac{\eta'((\tau+1)/2)}{\eta((\tau+1)/2)} \right) , \end{aligned} \quad (\text{A9})$$

where $\eta'(\tau)$ is first derivative w.r.t. τ and the expression of Dedekind eta-function $\eta(\tau)$ is given by

$$\eta(\tau) = q^{1/24} \prod_{n=1}^{\infty} (1 - q^n) , \quad q \equiv e^{2i\pi\tau} . \quad (\text{A10})$$

In the form of q -expansion, we can write modular Yukawas as follows ($y_i(\tau) \equiv y_i$)

$$\begin{aligned} y_1 &= \frac{1}{8} (1 + 24q + 24q^2 + 96q^3 + 24q^4 + 144q^5 + 96q^6 + 192q^7 + 24q^8 + 312q^9 + 144q^{10} + \dots) , \\ y_2 &= \sqrt{3}q^{1/2} (1 + 4q + 6q^2 + 8q^3 + 13q^4 + 12q^5 + 14q^6 + 24q^7 + 18q^8 + 20q^9 + \dots) . \end{aligned} \quad (\text{A11})$$

The higher modular weight Yukawas can be constructed from weight 2 Yukawas y_1 , y_2 , following the tensor product rules of S_3 provided in Eq. (A4). The modular Yukawas of

weight 4 and 6 are obtained as follows

$$Y_{\mathbf{1}}^{(4)} = y_1^2 + y_2^2, \quad Y_{\mathbf{1}'}^{(4)} = 0, \quad Y_{\mathbf{2}}^{(4)} = \begin{pmatrix} -y_1^2 + y_2^2 \\ 2y_1y_2 \end{pmatrix},$$

$$Y_{\mathbf{1}}^{(6)} = -y_1^3 + 3y_1y_2^2, \quad Y_{\mathbf{1}'}^{(6)} = -3y_1^2y_2 + y_2^3, \quad Y_{\mathbf{2}}^{(6)} = \begin{pmatrix} y_1^3 + y_1y_2^2 \\ y_1^2y_2 + y_2^3 \end{pmatrix}. \quad (\text{A12})$$

In a similar manner, the other higher modular weight Yukawa can be constructed following the tensor product rules of S_3 given in Eq. (A4).

- [1] **Kamiokande-II** Collaboration, K. S. Hirata *et al.*, “Results from one thousand days of real time directional solar neutrino data,” *Phys. Rev. Lett.* **65** (1990) 1297–1300.
- [2] **Kamiokande-II** Collaboration, K. S. Hirata *et al.*, “Observation of a small atmospheric muon-neutrino / electron-neutrino ratio in Kamiokande,” *Phys. Lett. B* **280** (1992) 146–152.
- [3] **Super-Kamiokande** Collaboration, Y. Fukuda *et al.*, “Evidence for oscillation of atmospheric neutrinos,” *Phys. Rev. Lett.* **81** (1998) 1562–1567, [arXiv:hep-ex/9807003](https://arxiv.org/abs/hep-ex/9807003).
- [4] B. T. Cleveland, T. Daily, R. Davis, Jr., J. R. Distel, K. Lande, C. K. Lee, P. S. Wildenhain, and J. Ullman, “Measurement of the solar electron neutrino flux with the Homestake chlorine detector,” *Astrophys. J.* **496** (1998) 505–526.
- [5] **SNO** Collaboration, Q. R. Ahmad *et al.*, “Direct evidence for neutrino flavor transformation from neutral current interactions in the Sudbury Neutrino Observatory,” *Phys. Rev. Lett.* **89** (2002) 011301, [arXiv:nucl-ex/0204008](https://arxiv.org/abs/nucl-ex/0204008).
- [6] **Planck** Collaboration, N. Aghanim *et al.*, “Planck 2018 results. VI. Cosmological parameters,” *Astron. Astrophys.* **641** (2020) A6, [arXiv:1807.06209 \[astro-ph.CO\]](https://arxiv.org/abs/1807.06209). [Erratum: *Astron. Astrophys.* 652, C4 (2021)].
- [7] E. Ma, “Verifiable radiative seesaw mechanism of neutrino mass and dark matter,” *Phys. Rev. D* **73** (2006) 077301, [arXiv:hep-ph/0601225 \[hep-ph\]](https://arxiv.org/abs/hep-ph/0601225).
- [8] N. Kumar, T. Nomura, and H. Okada, “Scotogenic neutrino mass with large $SU(2)_L$ multiplet fields,” *Eur. Phys. J. C* **80** no. 8, (2020) 801, [arXiv:1912.03990 \[hep-ph\]](https://arxiv.org/abs/1912.03990).
- [9] S.-Y. Guo and Z.-L. Han, “Observable Signatures of Scotogenic Dirac Model,” *JHEP* **12**

(2020) 062, [arXiv:2005.08287 \[hep-ph\]](https://arxiv.org/abs/2005.08287).

[10] J. Leite, A. Morales, J. W. F. Valle, and C. A. Vaquera-Araujo, “Scotogenic dark matter and Dirac neutrinos from unbroken gauged $B - L$ symmetry,” *Phys. Lett. B* **807** (2020) 135537, [arXiv:2003.02950 \[hep-ph\]](https://arxiv.org/abs/2003.02950).

[11] D. W. Kang, J. Kim, and H. Okada, “Muon g-2 in $U(1)\mu - \tau$ symmetric gauged radiative neutrino mass model,” *Phys. Lett. B* **822** (2021) 136666, [arXiv:2107.09960 \[hep-ph\]](https://arxiv.org/abs/2107.09960).

[12] T. Nomura and H. Okada, “Radiative neutrino mass model in dark non-Abelian gauge symmetry,” *Phys. Rev. D* **105** no. 7, (2022) 075010, [arXiv:2106.10451 \[hep-ph\]](https://arxiv.org/abs/2106.10451).

[13] D. Borah, P. Das, and D. Nanda, “Observable ΔN_{eff} in Dirac scotogenic model,” *Eur. Phys. J. C* **84** no. 2, (2024) 140, [arXiv:2211.13168 \[hep-ph\]](https://arxiv.org/abs/2211.13168).

[14] D. Borah, E. Ma, and D. Nanda, “Dark $SU(2)$ gauge symmetry and scotogenic Dirac neutrinos,” *Phys. Lett. B* **835** (2022) 137539, [arXiv:2204.13205 \[hep-ph\]](https://arxiv.org/abs/2204.13205).

[15] S. Chuliá Centelles, R. Cepedello, and O. Medina, “Absolute neutrino mass scale and dark matter stability from flavour symmetry,” *JHEP* **10** (2022) 080, [arXiv:2204.12517 \[hep-ph\]](https://arxiv.org/abs/2204.12517).

[16] T. Nomura and H. Okada, “Scotogenic models with a general lepton flavor dependent $U(1)$ gauge symmetry,” *Phys. Lett. B* **848** (2024) 138393, [arXiv:2304.03905 \[hep-ph\]](https://arxiv.org/abs/2304.03905).

[17] L. Singh, D. Mahanta, and S. Verma, “Low scale leptogenesis in singlet-triplet scotogenic model,” *JCAP* **02** (2024) 041, [arXiv:2309.12755 \[hep-ph\]](https://arxiv.org/abs/2309.12755).

[18] R. Kumar, N. Nath, and R. Srivastava, “Cutting the scotogenic loop: adding flavor to dark matter,” *JHEP* **12** (2024) 036, [arXiv:2406.00188 \[hep-ph\]](https://arxiv.org/abs/2406.00188).

[19] P. Bharadwaj, R. Kumar, H. K. Prajapati, R. Srivastava, and S. Yadav, “Dark Matter Escaping Direct Detection Runs into Higgs Mass Hierarchy Problem,” [arXiv:2412.13301 \[hep-ph\]](https://arxiv.org/abs/2412.13301).

[20] D. Borah, P. Das, B. Karmakar, and S. Mahapatra, “Discrete dark matter with light Dirac neutrinos,” *Phys. Rev. D* **111** no. 3, (2025) 035032, [arXiv:2406.17861 \[hep-ph\]](https://arxiv.org/abs/2406.17861).

[21] S. Centelles Chuliá, R. Srivastava, and S. Yadav, “Comprehensive phenomenology of the Dirac Scotogenic Model: Novel low-mass dark matter,” *JHEP* **04** (2025) 038, [arXiv:2409.18513 \[hep-ph\]](https://arxiv.org/abs/2409.18513).

[22] T. Nomura, H. Okada, and O. Popov, “Non-holomorphic modular A_4 symmetric scotogenic model,” *Phys. Lett. B* **860** (2025) 139171, [arXiv:2409.12547 \[hep-ph\]](https://arxiv.org/abs/2409.12547).

- [23] T. Nomura and O. Popov, “Extended scotogenic model of neutrino mass and proton decay,” *Phys. Rev. D* **110** no. 7, (2024) 075035, [arXiv:2406.00651 \[hep-ph\]](https://arxiv.org/abs/2406.00651).
- [24] L. Singh, R. Srivastava, S. Verma, and S. Yadav, “Type-III Scotogenic Model: Inflation, Dark Matter and Collider Phenomenology,” [arXiv:2501.13171 \[hep-ph\]](https://arxiv.org/abs/2501.13171).
- [25] V. M. Lozano, G. Sanchez Garcia, and J. W. F. Valle, “Collider signatures of fermionic scotogenic dark matter,” *Phys. Rev. D* **112** no. 5, (2025) 055007, [arXiv:2502.05270 \[hep-ph\]](https://arxiv.org/abs/2502.05270).
- [26] R. S. Hundi, “Lepton flavor violation in the Majorana and Dirac scotogenic models,” *Eur. Phys. J. C* **85** no. 7, (2025) 805, [arXiv:2502.04733 \[hep-ph\]](https://arxiv.org/abs/2502.04733).
- [27] S.-Y. Guo and M.-Y. Zhao, “Probing the Scotogenic Dirac Model with FIMP Dark Matter and ΔN_{eff} ,” [arXiv:2508.16362 \[hep-ph\]](https://arxiv.org/abs/2508.16362).
- [28] R. Kumar and R. Srivastava, “Dark Matter Induced Proton Decays,” [arXiv:2506.04370 \[hep-ph\]](https://arxiv.org/abs/2506.04370).
- [29] I. M. Ávila, A. Karan, S. Mandal, S. Sadhukhan, and J. W. F. Valle, “Dark matter as the source of neutrino mass: theory overview and experimental prospects,” [arXiv:2506.24027 \[hep-ph\]](https://arxiv.org/abs/2506.24027).
- [30] R. Kumar, N. Nath, R. Srivastava, and S. Yadav, “Dirac Scoto inverse-seesaw from A_4 flavor symmetry,” *JHEP* **10** (2025) 088, [arXiv:2505.01407 \[hep-ph\]](https://arxiv.org/abs/2505.01407).
- [31] A. AbuSiam and A. Ahriche, “The scotogenic model with two inert doublets: Parameter space and electroweak precision tests,” *Int. J. Mod. Phys. A* **40** no. 31, (2025) 2550157, [arXiv:2506.18051 \[hep-ph\]](https://arxiv.org/abs/2506.18051).
- [32] T. Nomura, H. Okada, and X.-Y. Wang, “A radiative neutrino mass model with leptoquarks under non-holomorphic modular A_4 symmetry,” *JHEP* **09** (2025) 163, [arXiv:2504.21404 \[hep-ph\]](https://arxiv.org/abs/2504.21404).
- [33] T. Nomura and O. Popov, “No-group Scotogenic Model,” [arXiv:2507.10299 \[hep-ph\]](https://arxiv.org/abs/2507.10299).
- [34] N. J. Jobu and K. Nishiwaki, “Z4 scotogenic model with a Higgs portal,” *Phys. Rev. D* **112** no. 11, (2025) 115009, [arXiv:2508.18713 \[hep-ph\]](https://arxiv.org/abs/2508.18713).
- [35] R. Kumar, H. K. Prajapati, R. Srivastava, and S. Yadav, “Flavor imprints on novel low mass dark matter,” *JHEP* **11** (2025) 094, [arXiv:2510.02972 \[hep-ph\]](https://arxiv.org/abs/2510.02972).
- [36] S. Nasri, L. Singh, Tapender, and S. Verma, “Dark-Portal Leptogenesis in a Non-Holomorphic Modular Scoto-Seesaw Model,” [arXiv:2601.06435 \[hep-ph\]](https://arxiv.org/abs/2601.06435).

- [37] C. A. Baker *et al.*, “An Improved experimental limit on the electric dipole moment of the neutron,” *Phys. Rev. Lett.* **97** (2006) 131801, [arXiv:hep-ex/0602020](https://arxiv.org/abs/hep-ex/0602020).
- [38] J. M. Pendlebury *et al.*, “Revised experimental upper limit on the electric dipole moment of the neutron,” *Phys. Rev. D* **92** no. 9, (2015) 092003, [arXiv:1509.04411 \[hep-ex\]](https://arxiv.org/abs/1509.04411).
- [39] R. D. Peccei and H. R. Quinn, “CP Conservation in the Presence of Instantons,” *Phys. Rev. Lett.* **38** (1977) 1440–1443.
- [40] R. D. Peccei and H. R. Quinn, “Constraints Imposed by CP Conservation in the Presence of Instantons,” *Phys. Rev. D* **16** (1977) 1791–1797.
- [41] S. Weinberg, “A New Light Boson?,” *Phys. Rev. Lett.* **40** (1978) 223–226.
- [42] F. Wilczek, “Problem of Strong P and T Invariance in the Presence of Instantons,” *Phys. Rev. Lett.* **40** (1978) 279–282.
- [43] J. E. Kim, “Weak Interaction Singlet and Strong CP Invariance,” *Phys. Rev. Lett.* **43** (1979) 103.
- [44] M. A. Shifman, A. I. Vainshtein, and V. I. Zakharov, “Can Confinement Ensure Natural CP Invariance of Strong Interactions?,” *Nucl. Phys. B* **166** (1980) 493–506.
- [45] A. R. Zhitnitsky, “On Possible Suppression of the Axion Hadron Interactions. (In Russian),” *Sov. J. Nucl. Phys.* **31** (1980) 260.
- [46] M. Dine, W. Fischler, and M. Srednicki, “A Simple Solution to the Strong CP Problem with a Harmless Axion,” *Phys. Lett. B* **104** (1981) 199–202.
- [47] A. Batra, H. B. Câmara, F. R. Joaquim, N. Nath, R. Srivastava, and J. W. F. Valle, “Axion framework with color-mediated Dirac neutrino masses,” *Phys. Lett. B* **868** (2025) 139629, [arXiv:2501.13156 \[hep-ph\]](https://arxiv.org/abs/2501.13156).
- [48] A. Batra, H. B. Câmara, F. R. Joaquim, R. Srivastava, and J. W. F. Valle, “Axion Paradigm with Color-Mediated Neutrino Masses,” *Phys. Rev. Lett.* **132** no. 5, (2024) 051801, [arXiv:2309.06473 \[hep-ph\]](https://arxiv.org/abs/2309.06473).
- [49] S. K. Kang and H. Okada, “Neutrino masses and mixing in an axion model,” *Eur. Phys. J. C* **85** no. 8, (2025) 917, [arXiv:2408.14942 \[hep-ph\]](https://arxiv.org/abs/2408.14942).
- [50] J. Preskill, M. B. Wise, and F. Wilczek, “Cosmology of the Invisible Axion,” *Phys. Lett. B* **120** (1983) 127–132.
- [51] L. F. Abbott and P. Sikivie, “A Cosmological Bound on the Invisible Axion,” *Phys. Lett. B* **120** (1983) 133–136.

- [52] M. Dine and W. Fischler, “The Not So Harmless Axion,” *Phys. Lett. B* **120** (1983) 137–141.
- [53] F. Feruglio, *Are neutrino masses modular forms?*, pp. 227–266. 2019. [arXiv:1706.08749](https://arxiv.org/abs/1706.08749) [hep-ph].
- [54] T. Kobayashi, K. Tanaka, and T. H. Tatsuishi, “Neutrino mixing from finite modular groups,” *Phys. Rev. D* **98** no. 1, (2018) 016004, [arXiv:1803.10391](https://arxiv.org/abs/1803.10391) [hep-ph].
- [55] D. Meloni and M. Parriciatu, “A simplest modular S_3 model for leptons,” [arXiv:2306.09028](https://arxiv.org/abs/2306.09028) [hep-ph].
- [56] H. Okada and Y. Orikasa, “Modular S_3 symmetric radiative seesaw model,” *Phys. Rev. D* **100** no. 11, (2019) 115037, [arXiv:1907.04716](https://arxiv.org/abs/1907.04716) [hep-ph].
- [57] S. Mishra, “Neutrino mixing and Leptogenesis with modular S_3 symmetry in the framework of type III seesaw,” [arXiv:2008.02095](https://arxiv.org/abs/2008.02095) [hep-ph].
- [58] M. K. Behera, P. Ittisamai, C. Pongkitivanichkul, and P. Uttayarat, “Neutrino phenomenology in the modular S_3 seesaw model,” *Phys. Rev. D* **110** no. 3, (2024) 035004, [arXiv:2403.00593](https://arxiv.org/abs/2403.00593) [hep-ph].
- [59] M. K. Behera, P. Ittisamai, C. Pongkitivanichkul, and P. Uttayarat, “Phenomenology of inverse seesaw using S_3 modular symmetry,” *Eur. Phys. J. C* **85** no. 11, (2025) 1316, [arXiv:2504.12954](https://arxiv.org/abs/2504.12954) [hep-ph].
- [60] Z. Tavartkiladze, “Minimal Modular Flavor Symmetry and Lepton Textures Near Fixed Points,” [arXiv:2512.24804](https://arxiv.org/abs/2512.24804) [hep-ph].
- [61] T. Nomura, H. Okada, and H. Otsuka, “Texture zeros realization in a three-loop radiative neutrino mass model from modular A_4 symmetry,” [arXiv:2309.13921](https://arxiv.org/abs/2309.13921) [hep-ph].
- [62] P. Mishra, M. K. Behera, P. Panda, and R. Mohanta, “Type III seesaw under A_4 modular symmetry with leptogenesis,” *Eur. Phys. J. C* **82** no. 12, (2022) 1115, [arXiv:2204.08338](https://arxiv.org/abs/2204.08338) [hep-ph].
- [63] X. Wang, “Lepton flavor mixing and CP violation in the minimal type-(I+II) seesaw model with a modular A_4 symmetry,” *Nucl. Phys. B* **957** (2020) 115105, [arXiv:1912.13284](https://arxiv.org/abs/1912.13284) [hep-ph].
- [64] M. Kashav and S. Verma, “Broken scaling neutrino mass matrix and leptogenesis based on A_4 modular invariance,” *JHEP* **09** (2021) 100, [arXiv:2103.07207](https://arxiv.org/abs/2103.07207) [hep-ph].
- [65] M. Kashav and S. Verma, “On minimal realization of topological Lorentz structures with one-loop seesaw extensions in A_4 modular symmetry,” *JCAP* **03** (2023) 010,

[arXiv:2205.06545 \[hep-ph\]](https://arxiv.org/abs/2205.06545).

- [66] P. Mishra, M. K. Behera, P. Panda, M. Ghosh, and R. Mohanta, “Exploring Models with Modular Symmetry in Neutrino Oscillation Experiments,” [arXiv:2305.08576 \[hep-ph\]](https://arxiv.org/abs/2305.08576).
- [67] J.-N. Lu, X.-G. Liu, and G.-J. Ding, “Modular symmetry origin of texture zeros and quark lepton unification,” *Phys. Rev. D* **101** no. 11, (2020) 115020, [arXiv:1912.07573 \[hep-ph\]](https://arxiv.org/abs/1912.07573).
- [68] M. Ricky Devi, “Neutrino Masses and Higher Degree Siegel Modular Forms,” [arXiv:2401.16257 \[hep-ph\]](https://arxiv.org/abs/2401.16257).
- [69] T. Kobayashi, T. Nomura, and T. Shimomura, “Type II seesaw models with modular A_4 symmetry,” *Phys. Rev. D* **102** no. 3, (2020) 035019, [arXiv:1912.00637 \[hep-ph\]](https://arxiv.org/abs/1912.00637).
- [70] T. Nomura, H. Okada, and S. Patra, “An inverse seesaw model with A_4 -modular symmetry,” *Nucl. Phys. B* **967** (2021) 115395, [arXiv:1912.00379 \[hep-ph\]](https://arxiv.org/abs/1912.00379).
- [71] M. K. Behera, S. Singirala, S. Mishra, and R. Mohanta, “A modular A_4 symmetric scotogenic model for neutrino mass and dark matter,” *J. Phys. G* **49** no. 3, (2022) 035002, [arXiv:2009.01806 \[hep-ph\]](https://arxiv.org/abs/2009.01806).
- [72] B. Mitesh Kumar, *Phenomenological aspects of modular symmetry on neutrino mass models*. PhD thesis, Hyderabad U., 2023.
- [73] T. Nomura and H. Okada, “Quark and lepton model with flavor specific dark matter and muon $g - 2$ in modular A_4 and hidden $U(1)$ symmetries,” [arXiv:2304.13361 \[hep-ph\]](https://arxiv.org/abs/2304.13361).
- [74] J. Kim and H. Okada, “Fermi-LAT GeV excess and muon $g - 2$ in a modular A_4 symmetry,” [arXiv:2302.09747 \[hep-ph\]](https://arxiv.org/abs/2302.09747).
- [75] X. K. Du and F. Wang, “Flavor structures of quarks and leptons from flipped SU(5) GUT with A_4 modular flavor symmetry,” *JHEP* **01** (2023) 036, [arXiv:2209.08796 \[hep-ph\]](https://arxiv.org/abs/2209.08796).
- [76] M. R. Devi, “Retrieving texture zeros in 3+1 active-sterile neutrino framework under the action of A_4 modular-invariants,” [arXiv:2303.04900 \[hep-ph\]](https://arxiv.org/abs/2303.04900).
- [77] A. Dasgupta, T. Nomura, H. Okada, O. Popov, and M. Tanimoto, “Dirac Radiative Neutrino Mass with Modular Symmetry and Leptogenesis,” [arXiv:2111.06898 \[hep-ph\]](https://arxiv.org/abs/2111.06898).
- [78] T. Nomura, H. Okada, and O. Popov, “A modular A_4 symmetric scotogenic model,” *Phys. Lett. B* **803** (2020) 135294, [arXiv:1908.07457 \[hep-ph\]](https://arxiv.org/abs/1908.07457).
- [79] S. Centelles Chuliá, R. Kumar, O. Popov, and R. Srivastava, “Neutrino Mass Sum Rules from Modular A_4 Symmetry,” [arXiv:2308.08981 \[hep-ph\]](https://arxiv.org/abs/2308.08981).
- [80] R. Kumar, P. Mishra, M. K. Behera, R. Mohanta, and R. Srivastava, “Predictions from

scoto-seesaw with A_4 modular symmetry,” *Phys. Lett. B* **853** (2024) 138635, [arXiv:2310.02363 \[hep-ph\]](https://arxiv.org/abs/2310.02363).

[81] T. Kobayashi, T. Nomura, H. Okada, and H. Otsuka, “Modular flavor models with positive modular weights: a new lepton model building,” *JHEP* **01** (2024) 121, [arXiv:2310.10091 \[hep-ph\]](https://arxiv.org/abs/2310.10091).

[82] T. Nomura and H. Okada, “Quasi two-zero texture in Type-II seesaw at fixed points from modular A_4 symmetry,” [arXiv:2407.13167 \[hep-ph\]](https://arxiv.org/abs/2407.13167).

[83] T. Nomura and H. Okada, “Lepton seesaw model in a modular A_4 symmetry,” [arXiv:2409.10912 \[hep-ph\]](https://arxiv.org/abs/2409.10912).

[84] T. Nomura and H. Okada, “A More Novel Approach of Radiative Linear Seesaw in a Modular A_4 Symmetry,” *PTEP* **2025** no. 4, (2025) 043B04, [arXiv:2410.21843 \[hep-ph\]](https://arxiv.org/abs/2410.21843).

[85] L. Singh, M. Kashav, and S. Verma, “Minimal type-I Dirac seesaw and leptogenesis under A_4 modular invariance,” *Nucl. Phys. B* **1007** (2024) 116666, [arXiv:2405.07165 \[hep-ph\]](https://arxiv.org/abs/2405.07165).

[86] G. Pathak, P. Das, and M. K. Das, “Neutrino mass genesis in scoto-inverse seesaw with modular A_4 ,” *Eur. Phys. J. C* **85** no. 5, (2025) 569, [arXiv:2411.13895 \[hep-ph\]](https://arxiv.org/abs/2411.13895).

[87] T. Nomura and H. Okada, “A new type of lepton seesaw model in a modular A_4 symmetry,” [arXiv:2503.19251 \[hep-ph\]](https://arxiv.org/abs/2503.19251).

[88] S. Centelles Chuliá and R. Kumar, “Minimal A_4 Type-II Seesaw Realization of Testable Neutrino Mass Sum Rules,” [arXiv:2512.22343 \[hep-ph\]](https://arxiv.org/abs/2512.22343).

[89] G. Pathak and M. K. Das, “Matter-antimatter asymmetry in minimal inverse seesaw framework with A_4 modular symmetry,” [arXiv:2505.03000 \[hep-ph\]](https://arxiv.org/abs/2505.03000).

[90] J. T. Penedo and S. T. Petcov, “Lepton Masses and Mixing from Modular S_4 Symmetry,” *Nucl. Phys. B* **939** (2019) 292–307, [arXiv:1806.11040 \[hep-ph\]](https://arxiv.org/abs/1806.11040).

[91] P. P. Novichkov, J. T. Penedo, S. T. Petcov, and A. V. Titov, “Modular S_4 models of lepton masses and mixing,” *JHEP* **04** (2019) 005, [arXiv:1811.04933 \[hep-ph\]](https://arxiv.org/abs/1811.04933).

[92] T. Kobayashi, Y. Shimizu, K. Takagi, M. Tanimoto, and T. H. Tatsuishi, “ A_4 lepton flavor model and modulus stabilization from S_4 modular symmetry,” *Phys. Rev. D* **100** no. 11, (2019) 115045, [arXiv:1909.05139 \[hep-ph\]](https://arxiv.org/abs/1909.05139). [Erratum: Phys.Rev.D 101, 039904 (2020)].

[93] X.-G. Liu, C.-Y. Yao, and G.-J. Ding, “Modular invariant quark and lepton models in double covering of S_4 modular group,” *Phys. Rev. D* **103** no. 5, (2021) 056013, [arXiv:2006.10722 \[hep-ph\]](https://arxiv.org/abs/2006.10722).

- [94] I. de Medeiros Varzielas, M. Levy, J. T. Penedo, and S. T. Petcov, “Quarks at the modular S_4 cusp,” [arXiv:2307.14410 \[hep-ph\]](https://arxiv.org/abs/2307.14410).
- [95] G.-J. Ding, S. F. King, and C.-Y. Yao, “Modular $S_4 \times SU(5)$ GUT,” *Phys. Rev. D* **104** no. 5, (2021) 055034, [arXiv:2103.16311 \[hep-ph\]](https://arxiv.org/abs/2103.16311).
- [96] S. F. King and Y.-L. Zhou, “Trimaximal TM₁ mixing with two modular S_4 groups,” *Phys. Rev. D* **101** no. 1, (2020) 015001, [arXiv:1908.02770 \[hep-ph\]](https://arxiv.org/abs/1908.02770).
- [97] P. P. Novichkov, J. T. Penedo, S. T. Petcov, and A. V. Titov, “Modular A_5 symmetry for flavour model building,” *JHEP* **04** (2019) 174, [arXiv:1812.02158 \[hep-ph\]](https://arxiv.org/abs/1812.02158).
- [98] G.-J. Ding, S. F. King, and X.-G. Liu, “Modular A_4 symmetry models of neutrinos and charged leptons,” *JHEP* **09** (2019) 074, [arXiv:1907.11714 \[hep-ph\]](https://arxiv.org/abs/1907.11714).
- [99] C. Bonilla, S. Centelles-Chuliá, R. Cepedello, E. Peinado, and R. Srivastava, “Dark matter stability and Dirac neutrinos using only Standard Model symmetries,” *Phys. Rev. D* **101** no. 3, (2020) 033011, [arXiv:1812.01599 \[hep-ph\]](https://arxiv.org/abs/1812.01599).
- [100] S. Centelles Chuliá, R. Cepedello, E. Peinado, and R. Srivastava, “Scotogenic dark symmetry as a residual subgroup of Standard Model symmetries,” *Chin. Phys. C* **44** no. 8, (2020) 083110, [arXiv:1901.06402 \[hep-ph\]](https://arxiv.org/abs/1901.06402).
- [101] R. Srivastava, C. Bonilla, and E. Peinado, “The role of residual symmetries in dark matter stability and the neutrino nature,” *LHEP* **2** no. 1, (2019) 124, [arXiv:1903.01477 \[hep-ph\]](https://arxiv.org/abs/1903.01477).
- [102] **Particle Data Group** Collaboration, M. Tanabashi *et al.*, “Review of Particle Physics,” *Phys. Rev. D* **98** no. 3, (2018) 030001.
- [103] R. Barbieri, L. J. Hall, and V. S. Rychkov, “Improved naturalness with a heavy Higgs: An Alternative road to LHC physics,” *Phys. Rev. D* **74** (2006) 015007, [arXiv:hep-ph/0603188](https://arxiv.org/abs/hep-ph/0603188).
- [104] I. Esteban, M. C. Gonzalez-Garcia, M. Maltoni, I. Martinez-Soler, J. P. Pinheiro, and T. Schwetz, “NuFit-6.0: updated global analysis of three-flavor neutrino oscillations,” *JHEP* **12** (2024) 216, [arXiv:2410.05380 \[hep-ph\]](https://arxiv.org/abs/2410.05380).
- [105] **DESI** Collaboration, A. G. Adame *et al.*, “DESI 2024 VI: cosmological constraints from the measurements of baryon acoustic oscillations,” *JCAP* **02** (2025) 021, [arXiv:2404.03002 \[astro-ph.CO\]](https://arxiv.org/abs/2404.03002).
- [106] E. K. Akhmedov, M. Lindner, E. Schnapka, and J. W. F. Valle, “Dynamical left-right symmetry breaking,” *Phys. Rev. D* **53** (1996) 2752–2780, [arXiv:hep-ph/9509255](https://arxiv.org/abs/hep-ph/9509255).
- [107] M. Malinsky, J. C. Romao, and J. W. F. Valle, “Novel supersymmetric SO(10) seesaw

mechanism,” *Phys. Rev. Lett.* **95** (2005) 161801, [arXiv:hep-ph/0506296](https://arxiv.org/abs/hep-ph/0506296).

[108] R. N. Mohapatra and J. W. F. Valle, “Neutrino Mass and Baryon Number Nonconservation in Superstring Models,” *Phys. Rev. D* **34** (1986) 1642.

[109] M. C. Gonzalez-Garcia and J. W. F. Valle, “Fast Decaying Neutrinos and Observable Flavor Violation in a New Class of Majoron Models,” *Phys. Lett. B* **216** (1989) 360–366.

[110] A. Jodidio *et al.*, “Search for Right-Handed Currents in Muon Decay,” *Phys. Rev. D* **34** (1986) 1967. [Erratum: *Phys. Rev. D* 37, 237 (1988)].

[111] **MEG** Collaboration, A. M. Baldini *et al.*, “Search for the lepton flavour violating decay $\mu^+ \rightarrow e^+ \gamma$ with the full dataset of the MEG experiment,” *Eur. Phys. J. C* **76** no. 8, (2016) 434, [arXiv:1605.05081 \[hep-ex\]](https://arxiv.org/abs/1605.05081).

[112] **COMET** Collaboration, R. Abramishvili *et al.*, “COMET Phase-I Technical Design Report,” *PTEP* **2020** no. 3, (2020) 033C01, [arXiv:1812.09018 \[physics.ins-det\]](https://arxiv.org/abs/1812.09018).

[113] **Belle** Collaboration, A. Abdesselam *et al.*, “Search for lepton-flavor-violating tau-lepton decays to $\ell\gamma$ at Belle,” *JHEP* **10** (2021) 19, [arXiv:2103.12994 \[hep-ex\]](https://arxiv.org/abs/2103.12994).

[114] **COMET** Collaboration, M. Moritsu, “Search for Muon-to-Electron Conversion with the COMET Experiment †,” *Universe* **8** no. 4, (2022) 196, [arXiv:2203.06365 \[hep-ex\]](https://arxiv.org/abs/2203.06365).

[115] T. Xing, C. Wu, H. Miao, H.-B. Li, W. Li, Y. Yuan, and Y. Zhang, “Search for Majoron at the COMET experiment*,” *Chin. Phys. C* **47** no. 1, (2023) 013108, [arXiv:2209.12802 \[hep-ex\]](https://arxiv.org/abs/2209.12802).

[116] **MEG II** Collaboration, K. Afanaciev *et al.*, “A search for $\mu^+ \rightarrow e^+ \gamma$ with the first dataset of the MEG II experiment,” *Eur. Phys. J. C* **84** no. 3, (2024) 216, [arXiv:2310.12614 \[hep-ex\]](https://arxiv.org/abs/2310.12614). [Erratum: *Eur. Phys. J. C* 84, 1042 (2024)].

[117] **Mu3e** Collaboration, A.-K. Perrevoort, “Charged lepton flavour violation - Overview of current experimental limits and future plans,” *PoS DISCRETE2022* (2024) 015.

[118] W. C. Haxton and E. Rule, “Distinguishing Charged Lepton Flavor Violation Scenarios with Inelastic $\mu \rightarrow e$ Conversion,” *Phys. Rev. Lett.* **133** no. 26, (2024) 261801, [arXiv:2404.17166 \[hep-ph\]](https://arxiv.org/abs/2404.17166).

[119] **Mu2e** Collaboration, D. Palo, “Charged Lepton Flavor Violating Experiments with Muons,” in *29th International Symposium on Particles, String and Cosmology*. 5, 2025. [arXiv:2505.04764 \[hep-ex\]](https://arxiv.org/abs/2505.04764).

[120] **BaBar** Collaboration, B. Aubert *et al.*, “Searches for Lepton Flavor Violation in the Decays

$\tau^\pm \rightarrow e^\pm \gamma$ and $\tau^\pm \rightarrow \mu^\pm \gamma$,” *Phys. Rev. Lett.* **104** (2010) 021802, [arXiv:0908.2381 \[hep-ex\]](https://arxiv.org/abs/0908.2381).

- [121] G. Grilli di Cortona, E. Hardy, J. Pardo Vega, and G. Villadoro, “The QCD axion, precisely,” *JHEP* **01** (2016) 034, [arXiv:1511.02867 \[hep-ph\]](https://arxiv.org/abs/1511.02867).
- [122] L. Di Luzio, M. Giannotti, E. Nardi, and L. Visinelli, “The landscape of QCD axion models,” *Phys. Rept.* **870** (2020) 1–117, [arXiv:2003.01100 \[hep-ph\]](https://arxiv.org/abs/2003.01100).
- [123] L. Visinelli and P. Gondolo, “Dark Matter Axions Revisited,” *Phys. Rev. D* **80** (2009) 035024, [arXiv:0903.4377 \[astro-ph.CO\]](https://arxiv.org/abs/0903.4377).
- [124] M. Kawasaki, K. Saikawa, and T. Sekiguchi, “Axion dark matter from topological defects,” *Phys. Rev. D* **91** no. 6, (2015) 065014, [arXiv:1412.0789 \[hep-ph\]](https://arxiv.org/abs/1412.0789).
- [125] R. T. Co, L. J. Hall, and K. Harigaya, “Axion Kinetic Misalignment Mechanism,” *Phys. Rev. Lett.* **124** no. 25, (2020) 251802, [arXiv:1910.14152 \[hep-ph\]](https://arxiv.org/abs/1910.14152).
- [126] E. Armengaud *et al.*, “Conceptual Design of the International Axion Observatory (IAXO),” *JINST* **9** (2014) T05002, [arXiv:1401.3233 \[physics.ins-det\]](https://arxiv.org/abs/1401.3233).
- [127] I. Stern, “ADMX Status,” *PoS ICHEP2016* (2016) 198, [arXiv:1612.08296 \[physics.ins-det\]](https://arxiv.org/abs/1612.08296).
- [128] S. Beurthey *et al.*, “MADMAX Status Report,” [arXiv:2003.10894 \[physics.ins-det\]](https://arxiv.org/abs/2003.10894).
- [129] Y. K. Semertzidis *et al.*, “Axion Dark Matter Research with IBS/CAPP,” [arXiv:1910.11591 \[physics.ins-det\]](https://arxiv.org/abs/1910.11591).
- [130] C. A. J. O’Hare, “Cosmology of axion dark matter,” *PoS COSMICWISPers* (2024) 040, [arXiv:2403.17697 \[hep-ph\]](https://arxiv.org/abs/2403.17697).
- [131] J. W. Foster, S. J. Witte, M. Lawson, T. Linden, V. Gajjar, C. Weniger, and B. R. Safdi, “Extraterrestrial Axion Search with the Breakthrough Listen Galactic Center Survey,” *Phys. Rev. Lett.* **129** no. 25, (2022) 251102, [arXiv:2202.08274 \[astro-ph.CO\]](https://arxiv.org/abs/2202.08274).
- [132] M. H. Chan, “Constraining the axion–photon coupling using radio data of the Bullet cluster,” *Sci. Rep.* **11** no. 1, (2021) 20087, [arXiv:2109.11734 \[astro-ph.CO\]](https://arxiv.org/abs/2109.11734).
- [133] A. Ayala, I. Domínguez, M. Giannotti, A. Mirizzi, and O. Straniero, “Revisiting the bound on axion–photon coupling from Globular Clusters,” *Phys. Rev. Lett.* **113** no. 19, (2014) 191302, [arXiv:1406.6053 \[astro-ph.SR\]](https://arxiv.org/abs/1406.6053).
- [134] CAST Collaboration, V. Anastassopoulos *et al.*, “New CAST Limit on the Axion-Photon Interaction,” *Nature Phys.* **13** (2017) 584–590, [arXiv:1705.02290 \[hep-ex\]](https://arxiv.org/abs/1705.02290).

- [135] C. A. Manzari, Y. Park, B. R. Safdi, and I. Savoray, “Supernova Axions Convert to Gamma Rays in Magnetic Fields of Progenitor Stars,” *Phys. Rev. Lett.* **133** no. 21, (2024) 211002, [arXiv:2405.19393 \[hep-ph\]](https://arxiv.org/abs/2405.19393).
- [136] R. de Adelhart Toorop, F. Feruglio, and C. Hagedorn, “Finite Modular Groups and Lepton Mixing,” *Nucl. Phys. B* **858** (2012) 437–467, [arXiv:1112.1340 \[hep-ph\]](https://arxiv.org/abs/1112.1340).